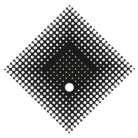
VICTORIA UNIVERSITY
MELBOURNE AUSTRALIA

Local-global interaction buckling of square high strength concrete-filled double steel tubular slender beam-columns

This is the Accepted version of the following publication

Ahmed, Mizan, Liang, Qing, Patel, Vipulkumar Ishvarbhai and Hadi, Muhammad NS (2019) Local-global interaction buckling of square high strength concrete-filled double steel tubular slender beam-columns. Thin-Walled Structures, 143. ISSN 0263-8231

The publisher's official version can be found at
https://www.sciencedirect.com/science/article/pii/S0263823118315982
Note that access to this version may require subscription.

Downloaded from VU Research Repository https://vuir.vu.edu.au/39333/

Ahmed, M., Liang, Q. Q., Patel, V. I. and Hadi, M. N. S. (2019). Local-global interaction buckling of square high strength concrete-filled double steel tubular slender beam-columns. *Thin-Walled Structures*, 143: 106244

Local-global interaction buckling of square high strength concrete-filled double steel tubular slender beam-columns

Mizan Ahmed[a], Qing Quan Liang[a,*], Vipulkumar Ishvarbhai Patel[b], Muhammad N. S. Hadi[c]

[a] *College of Engineering and Science, Victoria University, PO Box 14428, Melbourne, VIC 8001, Australia*
[b] *School of Engineering and Mathematical Sciences, La Trobe University, Bendigo, VIC 3552, Australia*
[c] *School of Civil, Mining and Environmental Engineering, University of Wollongong, Wollongong, NSW 2522, Australia*

ABSTRACT

High-strength square concrete-filled double steel tubular (CFDST) slender beam-columns with a circular internal steel tube subjected to eccentric loads may undergo interaction local-global buckling. No computational studies on the interaction local-global buckling of slender square CFDST beam-columns have been reported and their behavior has not been fully understood. This paper describes a mathematical model for the simulation of the interaction local-global buckling behavior of square high-strength CFDST slender beam-columns under axial compression in combination with uniaxial bending. The mathematical model is formulated by the fiber approach, accounting for confinement provided by the internal circular steel tube, and geometric and material nonlinearities. An incremental-iterative numerical procedure is designed to quantify the local-global interaction buckling responses of slender CFDST columns. Efficient numerical solution algorithms implementing the inverse quadratic method are developed for solving the nonlinear equilibrium dynamic functions of CFDST columns. The formulation proposed is verified by existing experimental data on CFDST columns as well as

*Corresponding author. Tel.: 61 3 9919 4134.
E-mail address: Qing.Liang@vu.edu.au (Q. Q. Liang)

double-skin concrete-filled steel tubular (DCFST) slender columns. The developed computational model is employed to study the local-global interaction buckling behavior of CFDST columns made of high-strength materials with various important parameters. Simplified design models are proposed for determining the ultimate axial strengths of slender square CFDST columns under axial compression and the interaction curves of CFDST slender beam-columns loaded eccentrically. It is demonstrated that the computational and design models predict well the interaction local-global buckling behavior and strength of slender square CFDST beam-columns.

Keywords: Concrete-filled double steel tubes; high-strength; slender beam-columns; local-global interaction buckling; nonlinear analysis.

1. Introduction

The applications of concrete-filled double steel tubular (CFDST) beam-columns made of high strength materials in tall buildings have been increased in recent years. The CFDST square columns as depicted in Fig. 1(a) combine the advantage properties of concrete and steel materials. In addition, CFDST columns offer improved ductility, stiffness, strength, and fire-resistance in comparison with square concrete-filled steel tubular (CFST) columns. The cross-sectional sizes of CFDST columns can be reduced by means of using high-strength steel and concrete and this greatly increases the space usage in composite buildings. A column having a slenderness ratio (L/r) greater than 22 is defined as a slender column in AS 3600-2009 [1]. Eccentrically loaded slender square CFDST thin-walled beam-columns may encounter the problem of local-global interaction instability. The nonlinear analysis and design of slender square CFDST columns under combined actions are complicated as the formulation must

consider the material nonlinearities, second-order effects as well as the interaction of local-global buckling. However, no attempt has been made to computationally investigate the inelastic responses of slender square high-strength CFDST columns loaded eccentrically, incorporating the interaction local-global buckling. To bridge this knowledge gap, a computationally-efficient mathematical model needs to be developed.

Experimental investigations on the strength and behavior of slender CFST columns with rectangular and square sections made of high-strength materials were carried out by researchers in the past. Varma et al. [2] conducted testes on slender high-strength CFST beam-columns which were subjected to constant axial load in combination with monotonically increasing moment. The steel tubes were made of either high-strength or normal strength steel and had the width-to-thickness ratio (b/t) of either 32 or 48. These columns were fabricated by using high-strength concrete of 110 MPa. It was shown that slender CFST square columns failed by the local-global interaction buckling with concrete crushing. The axial load and b/t ratio had remarkable effects on the column curvature ductility. The responses of square slender CFST columns loaded eccentrically to failure were studied experimentally by Mursi and Uy [3]. The steel tubes had the b/t ratios of 36, 46.4 and 56.8 and were filled with 60 MPa concrete. Mursi and Uy [4] undertook further tests on eccentrically-loaded square slender CFST columns constructed by steel tubes having a yield stress of 761 MPa and 20 MPa concrete. It was reported that the failure mode associated with slender CFST square columns was the global column buckling coupled with outward local buckling. The behavior of high-strength CFST rectangular columns that were loaded eccentrically to failure was experimentally studied by Liu [5]. Steel tubes having 550 MPa yield stress and high-strength concrete of either 70.8 MPa or 82.1 MPa were used to construct these columns. Liu [5] reported that the failure of CFST slender columns was caused by the outward local buckling and concrete crushing coupled with

overall column buckling. More recently, Du et al. [6, 7] carried out an experimental research on eccentrically loaded slender CFST columns with rectangular sections, incorporating *b*/*t* ratios of high-strength steel tubes ranging from 21 to 42.6. The observed failure modes of rectangular slender CFST columns with high-strength steel tubes were the column global buckling, local buckling, concrete crushing, and weld cracking.

The performance of double-skin CFST (DCFST) columns with hollow inner tube as depicted in Fig. 1(b) has been studied by Tao et al. [8, 9], Zhao et al. [10, 11] and Han et al. [12, 13]. Square DCFST slender columns under combined actions and DCFST members under cyclic loading were tested to failure by Han et al. [12,13]. The parameters chosen for the study included the member slenderness, loading eccentricity, and the section hollow ratio. Han et al. [12] also developed a theoretical model for quantifying the structural behavior of sqaure DCFST slender columns loaded uniaxially. Moreover, a simplified method for calculating the design strentgths of DCFST columns was proposed. Xiong et al. [14] performed tests on square CFST and DCFST slender columns incorporating an inner square steel tube. It was observed that the incorporation of an internal steel tube improved the ultimate strength of CFST columns.

Only limited experiments on the responses of CFDST columns having square outer sections were performed by Pei [15], Qian et al. [16-18], Xiong et al.[14, 19], and Wang et al. [20]. Pei [15] reported that short square CFDST columns failed by the outward local buckling of the outer square steel tubes while slender square CFDST columns failed by the local-global interaction buckling. The concrete with cube compressive strength up to 103 MPa was used to construct CFDST short columns by Qian et al. [17, 18]. The inner circular steel tube was found to provide an effective confinement to the concrete core, which resulted in improved ductility of the tested columns as well as their strengths. The residual strengths of the tested columns

were found to be about 75% of their ultimate axial strengths. Xiong et al. [14] tested one circular and one rectangular CFDST slender column under eccentric loading. The aforementioned tests showed that for the same design parameters, the ultimate strength of CFDST slender columns was higher than that of conventional CFST and DCFST slender columns.

The inelastic analysis procedures were utilized to simulate the structural responses of slender CFST rectangular and square columns [21-24]. Shanmugam et al. [21] proposed a theoretical formulation for the determination of the axial load-buckling performance of slender CFST columns with either slender or non-compact sections where local buckling occurs. A numerical model was described by Mursi and Uy [3, 4] that predicted the strength of slender thin-walled CFST rectangular columns loaded eccentrically about one principal axis and including local buckling. However, the numerical model given by Mursi and Uy [3, 4] employed the expressions for the effective widths of steel plates subjected to uniform stresses, which are not applicable to steel webs in CFST columns with rectangular sections under non-uniform stresses induced by uniaxial bending. Moreover, their model did not consider the progressive post-local buckling. Patel et al. [23] and Liang et al. [24] proposed fiber-based mathematical models for the predictions of local-global interaction buckling behavior of CFST rectangular columns which were designed to support axial compression as well as uniaxial or biaxial bending. The mathematical models were shown to be capable of simulating the gradual post-local buckling of steel tube walls under non-uniform stresses. Du et al. [6, 7] and Xiong et al. [14] employed the finite-element (FE) program ABAQUS to analyze rectangular CFST slender columns loaded eccentrically without the consideration of local buckling.

Computational research into the behavior of slender and short CFDST columns with rectangular section has been very limited. The FE models were created by Pei [15] and Wang et al. [20]

using the commercial FE software ABAQUS for analyzing nonlinear square CFDST short columns. The computer modeling technique using fiber approach proposed by Ahmed et al. [25] for short CFDST rectangular columns made of high-strength materials loaded concentrically incorporated the influences of confinement as well as the local buckling of the outer steel tube. Lü and Zhao [26] presented an analytical method for the simulation of nonlinear slender CFDST columns with square outer sections. The influences of the member slenderness, loading eccentricity as well as the outer tube thickness on the load-deflection behavior were studied. However, the aforementioned numerical models have not considered the influences of the interaction local-global buckling on the performance of CFDST slender columns made of square sections.

This paper extends the mathematical model proposed by Ahmed et al. [25] to the simulation of slender square high-strength CFDST beam-columns loaded eccentrically, including the interaction local-global buckling. The confinement effect induced by steel tubes is considered in the stress-strain relations of concrete. The theory and computational procedures for the calculations of the interaction local-global buckling responses of square CFDST columns under uniaxial bending and axial compression are described. Efficient numerical solution algorithms are developed for obtaining solutions to the nonlinear equilibrium dynamic functions. The validation of the computational modeling method against experimental data and parametric studies are conducted and discussed. Design models are proposed for estimating the ultimate strengths of slender square CFDST columns under axial compression and interaction curves of CFDST slender columns.

2. Formulation of the mathematical model

2.1. Inelastic analysis of cross-sections including local buckling

The mathematical model simulating the inelastic buckling of slender square CFDST columns is formulated by the method of fiber elements [27-30]. Figure 2 illustrates the typical mesh of fibers and the distribution of strain in the cross-section of a square CFDST column. The mesh generator developed by Persson and Strang [31] is used to discretize the sandwiched concrete while the discretization of the core concrete is similar to that of circular CFDST columns [29, 32] . It is assumed that the plane section remains plane after deformation. This results in a linear strain distribution through the depth of the cross-section as depicted in Fig. 2. The perfect bond between steel and concrete is assumed. These assumptions ensure that the strain compatibility in the cross-section throughout the loading history is achieved [29, 30]. The stresses of fibers are computed from fiber strains by the stress-strain relations of concrete and steel. Under combined actions, the fiber strain is calculated using the function of curvature (ϕ) and neutral axis depth (d_n) as shown in Fig. 2 [27]. The internal axial force (P) and moment (M) are calculated by integrating fiber stresses over the cross-section as stress resultants [27].

The steel tubular walls restrained by concrete in a rectangular CFDST column are susceptible to the outward local buckling. The ultimate strength of CFDST columns is reduced considerably by local buckling [27, 28]. The outward local-buckling is included in the present numerical modeling of square CFDST columns to accurately predict their inelastic behavior. The external steel flange and webs of a square CFDST column subjected to axial load in combination with bending about one principal axis are under either non-uniform or uniform stresses. Liang et al. [33] derived expressions that determine the initial local-buckling stresses of steel tube walls of CFST columns under non-uniform stresses. Experiments [15, 17, 18] indicated that the outer steel tube of a square CFDST column buckled locally outward, which is similar to that of a

conventional CFST column. Therefore, the expressions proposed by Liang et al. [33] are implemented directly in the present mathematical modeling procedures for CFDST columns. The progressive post-local buckling of steel tubes is modeled by gradually redistributing the in-plane stresses in the buckled walls. For this purpose, the effective width expressions of Liang et al. [33] are utilized. The effective widths b_{e1} and b_{e2} of the steel tube walls in a square CFDST column subjected to axial compression in addition to uniaxial bending are illustrated in Fig. 3, and are quantified by the following equations formulated by Liang et al. [33]:

$$\frac{b_{e1}}{b}=\begin{cases}0.2777+0.01019\left(\dfrac{b}{t_o}\right)-1.972\times10^{-4}\left(\dfrac{b}{t_o}\right)^2+9.605\times10^{-7}\left(\dfrac{b}{t_o}\right)^3 & (\alpha_s>0.0)\\ 0.4186+0.002047\left(\dfrac{b}{t_o}\right)+5.355\times10^{-5}\left(\dfrac{b}{t_o}\right)^2-4.685\times10^{-7}\left(\dfrac{b}{t_o}\right)^3 & (\alpha_s=0.0)\end{cases} \tag{1}$$

$$\frac{b_{e2}}{b}=(2-\alpha_s)\frac{b_{e1}}{b} \tag{2}$$

where b denotes the clear width of the external steel tube wall as presented in Fig. 3, t_o represents the outer tube thickness, α_s is the stress-gradient coefficient, which is taken $\alpha_s=\sigma_2/\sigma_1$, where σ_2 and σ_1 represent the minimum and maximum edge stressed on the plate, respectively.

The maximum ineffective width ($b_{ne,\max}$) of a steel plate corresponding to the ultimate axial load applied is determined as $(b-b_{e1}-b_{e2})$. The ineffective width (b_{ne}) between zero and $b_{ne,\max}$ is computed by means of the linear interpolation approach based on the steel fiber stress level, which can be written as

$$b_{ne} = \left(\frac{\sigma_1 - \sigma_{cr}}{f_{syo} - \sigma_{cr}} \right) b_{ne,\max} \tag{3}$$

in which σ_{cr} stands for the stress at the onset of the initial local-buckling of the outer steel tube wall, and f_{syo} represents the yield strength of the external steel tube.

The modeling scheme developed by Liang [27] for the progressive post-local buckling characterized by thin steel plates is used in the present computational modeling approach to incorporate post-local buckling into the global buckling simulation of CFST slender square columns.

2.2. Incremental-iterative global buckling analysis

A mathematical model is formulated for simulating the interaction local-global buckling responses of slender CFDST columns of square sections under uniaxial bending as well as axial compression. The formulation extends the numerical models proposed by Liang [34], Patel et al. [23] and Liang et al. [24] for conventional CFST slender columns to the simulation of slender CFDST columns. It should be noted that in the fiber analysis, the strain compatibility is used to control the deformations of the adjacent fiber elements while the displacement shape function is employed to control the overall deflection of the column. Unlike the finite element method, the computational model using the method of fiber elements does not need to use contact elements to model the interface of steel tube and concrete. Figure 4 illustrates the schematic view of the pin-ended CFDST slender column having equal loading eccentricity (*e*) and under single curvature bending. The column deflected shape is a part of a sinewave. The curvature at the column mid-length (ϕ_m) is obtained from the buckling shape function [34] as

$$\phi_m = u_m \left(\frac{\pi}{L} \right)^2 \tag{4}$$

where u_m stands for the buckling displacement/lateral deflection that occurs at the mid-length of the column, and L is the effective length of the pin-ended column.

The geometric imperfection (u_o) initially presented in the column and the second-order effect induced by the interaction of the axial load and buckling displacement (u_m) are included in the formulation. The external moment at the column mid-length is computed by

$$M_{ext} = P\left(e + u_m + u_o\right) \tag{5}$$

The default initial geometric imperfection (u_o) at the column mid-height is taken as L/1000 in the mathematical model. The global buckling analysis of square CFDST slender columns is formulated by means of employing the displacement-control method. The computational method incrementally increases the buckling displacement (u_m) at the mid-length of the column and calculates the internal axial force (P) and moment (M) considering local buckling effects [23, 24]. The internal axial force satisfying the equilibrium condition of moment at the column mid-height is treated as the axial load applied at the column ends. The complete axial load-buckling displacement curve for the slender CFDST column can be computed by iteratively executing this computational process.

In the calculations by the numerical method, the equilibrium condition at the column mid-height is satisfied if the following residual moment is sufficiently small:

$$r_p = M - P\left(e + u_m + u_o\right) \tag{6}$$

In mathematical form, the equilibrium condition is achieved if $\left|r_p\right| < \varepsilon_k = 10^{-4}$. The computer flowchart for the computation of the axial load-buckling displacement curve of slender CFST columns made of square sections is depicted in Fig. 5.

2.3. Solution algorithms implementing the inverse quadratic method

In the global buckling analysis of a slender column, the depth of the neutral axis of the section is iteratively adjusted to achieve the force and moment equilibrium at the mid-length of the column. The residual moment function (r_p) is changing in the computational process and is a highly nonlinear dynamic function, which is not derivative with respect to variables. Numerical solution algorithms implementing the secant approach and Müller's method have been programed by Liang [34], Patel et al. [23] and Liang et al. [24] for determining the neutral axis-depth. Although the secant and Müller's methods are effective numerical techniques for finding the roots of nonlinear functions, they are not used in the present study. Efficient numerical algorithms using the inverse quadratic method are developed to solve the dynamic functions. The solution algorithms developed in the present study are completely different from those presented by Liang [34], Patel et al. [23] and Liang et al. [24]. The inverse quadratic method requires three initial values to be assigned to the neutral axis depths $d_{n,1}$, $d_{n,2}$ and $d_{n,3}$ to facilitate the computation. The following equations are programed to adjust the neutral axis depth d_n:

$$d_{n,j+3} = d_{n,j+1} - r_{p,j+1}\left(\frac{A}{C}\right) \tag{7}$$

$$A=(r_{p,j})^2(d_{n,j+2}-d_{n,j+1})+r_{p,j}r_{p,j+1}(d_{n,j+1}-d_{n,j+2})+(r_{p,j+1}-r_{p,j+2})r_{p,j+2}(d_{n,j}-d_{n,j+1}) \quad (8)$$

$$C=\left(r_{p,j+1}-r_{p,j}\right)\left(r_{p,j+2}-r_{p,j}\right)\left(r_{p,j+2}-r_{p,j+1}\right) \quad (9)$$

where j is the iteration number. The iteration of searching for the true neutral axis depth d_n continues until the criterion of convergence $\left|r_p\right| < \varepsilon_k = 10^{-4}$ is satisfied. The prescribed value for the convergence criterion is sufficiently small that the solutions obtained are adequate for engineering purpose.

In the numerical analysis, the initial depths of the neutral axis are taken as $d_{n,1}=D_0, d_{n,2}=D_0/2$ and $d_{n,3}=\left(d_{n,1}+d_{n,2}\right)/2$. The inverse quadratic method is found to be very fast and efficient to determine the neutral axis depth of CFDST columns considering local buckling.

3. Stress-strain relations of structural steels

The three-stage stress-strain relations of structural steels presented in Fig. 6 consider the reduction of the steel yield strength as a result of biaxial stresses on the steel tube under compression. The rounded-part of the stress-strain curves is defined by the equation proposed by Liang [27]. The model for describing the strain-hardening behavior of structural steels by Mander [35] is adopted in the present numerical model, and is different from that used by Liang [34], Patel et al. [23] and Liang et al. [24]. The model by Mander [35] is expressed as

$$\sigma_s = f_{su} - \left(\frac{\varepsilon_{su}-\varepsilon_s}{\varepsilon_{su}-\varepsilon_{st}}\right)^n (f_{su}-f_{sy}) \quad \text{for } \varepsilon_{st} < \varepsilon_s \le \varepsilon_{su} \quad (10)$$

where σ_s and ε_s denote the longitudinal steel stress and corresponding strain, respectively; f_{sy} is the steel yield strength at the yield strain ε_{sy}; ε_{st} and ε_{su} represent the hardening strain and ultimate strain taken as 0.005 and 0.2, respectively. The strain-hardening exponent n is determined as

$$n = E_{st}\left(\frac{\varepsilon_{su} - \varepsilon_{st}}{f_{su} - f_{sy}}\right) \tag{11}$$

in which E_{st} is taken as $0.02E_s$, where E_s represents the Young's modulus of steel.

4. Stress-strain relations of confined concrete

4.1. General stress-strain curve

The two-stage constitutive laws of confined and unconfined concrete under compression are given in Fig 7. The ascending part of the stress-strain curve is expressed by using the following expression of Mander et al. [36]:

$$\sigma_c = \frac{f_{cc}^{'}(\varepsilon_c / \varepsilon_{cc}^{'})\lambda}{(\varepsilon_c / \varepsilon_{cc}^{'})^{\lambda} + \lambda - 1} \tag{12}$$

in which σ_c and ε_c denote the longitudinal concrete stress and corresponding strain, respectively; $f_{cc}^{'}$ and $\varepsilon_{cc}^{'}$ are the ultimate compressive strength and corresponding strain of confined concrete, respectively; the parameter λ is given as

$$\lambda = \frac{E_c \varepsilon_{cc}^{'}}{E_c \varepsilon_{cc}^{'} - f_{cc}^{'}} \tag{13}$$

$$E_c = 4400\sqrt{\gamma_c f_c^{'}} \quad \text{(MPa)} \tag{14}$$

in which γ_c was proposed by Liang [27] as $1.85 D_c^{-0.135}$ to consider the column size effects, and D_c is calculated as $(B_o - 2t_o)$.

The descending branch of the stress-strain curves given in Fig. 7 defines the post-peak responses of concrete. The equation presented by Lim and Ozbakkaloglu [37] is used to describe the descending branch in the present computational model and is completely different from those employed by Liang [34], Patel et al. [23] and Liang et al. [24]. The equation of Lim and Ozbakkaloglu [37] is written as

$$\sigma_c = f_{cc}^{'} - \frac{f_{cc}^{'} - f_{cr}}{\left[1 + \left(\frac{\varepsilon_c - \varepsilon_{cc}^{'}}{\varepsilon_{ci} - \varepsilon_{cc}^{'}}\right)^{-2}\right]} \tag{15}$$

in which f_{cr} represents the concrete residual strength and ε_{ci} stands for the strain that defines the inflection point.

4.2. Compressive strength and strain of confined concrete

The lateral pressure exerted by the circular inner steel tube to the core-concrete improves the ductility as well as the compressive strength of concrete [32]. This effect is considered in the constitutive relationships by quantifying the lateral pressure on the concrete using the formula

suggested by Lim and Ozbakkaloglu [37]. Ahmed et al. [25] modified the original expression to consider the column size effects (γ_c) as follows:

$$f_{cc}^{'} = 5.2\,(\gamma_c f_c^{'})^{0.91}\left(\frac{f_{rp}}{\gamma_c f_c^{'}}\right)^{a} + \gamma_c f_c^{'} \tag{16}$$

where $a = (\gamma_c f_c^{'})^{-0.06}$, and f_{rp} stands for the lateral pressure on the core-concrete.

The compressive concrete strain $\varepsilon_{cc}^{'}$ is calculated by

$$\varepsilon_{cc}^{'} = \varepsilon_c^{'} + 0.045\left(\frac{f_{rp}}{\gamma_c f_c^{'}}\right)^{1.15} \tag{17}$$

$$\varepsilon_c^{'} = \frac{(\gamma_c f_c^{'})^{0.225}}{1000} \tag{18}$$

where $\varepsilon_c^{'}$ is the strain corresponding to $\gamma_c f_c^{'}$.

As discussed by Wang et al. [20], the confinement induced by the external square steel tube to the sandwiched-concrete is so small that the lateral pressure (f_{rpo}) on the sandwiched concrete is assumed to be zero as suggested by Ahmed et al. [25]. However, the core-concrete is passively confined by the circular inner steel tube. The confining-pressure (f_{rpi}) on the core-concrete is estimated using the expressions of Liang and Fragomeni [38] based on the work of Hu et al. [39] and Tang et al. [40], which are written as

$$f_{rpi} = \begin{cases} 0.7\left(v_e - v_s\right)\left(\dfrac{2t_i}{D_i - 2t_i}\right) f_{syi} & \text{for } \dfrac{D_i}{t_i} \le 47 \\ \left(0.006241 - 0.0000357\dfrac{D_i}{t_i}\right) f_{syi} & \text{for } 47 < \dfrac{D_i}{t_i} \le 150 \end{cases} \tag{19}$$

in which v_e and v_s stand for the Poisson's ratios of the concrete-filled steel tube and of the hollow tube, respectively, and are given by Tang et al. [40].

4.3. Residual concrete strength and inflection point

The accurate determination of the residual concrete strength (f_{cr}) and the concrete strain (ε_{ci}) at the inflection point is vital to the accurate prediction of the post-peak behavior of square CFDST columns. The residual strength (f_{cr}) of the core-concrete is estimated by the expressions of Lim and Ozbakkaloglu [37] , written as

$$f_{cr} = \begin{cases} f_{cc}^{'} & \text{for } \dfrac{D_i}{t_i} \le 40 \\ 1.6 f_{cc}^{'}\left(\dfrac{f_{rpi}^{0.24}}{(\gamma_c f_c^{'})^{0.32}}\right) \text{ and } f_{cr} \le f_{cc}^{'} - 0.15\,(\gamma_c f_c^{'}) & \text{for } 40 < \dfrac{D_i}{t_i} \le 150 \end{cases} \tag{20}$$

On the other hand, the residual concrete strength (f_{cr}) of the sandwiched concrete is determined as $f_{cr} = \beta_c f_c^{'}$ where β_c is the strength degradation parameter for the sandwiched concrete. Ahmed et al. [25] proposed β_c based on the test results as

$$\beta_c = \begin{cases} 1 & \text{for } 0 \le \dfrac{B_o}{t_o} \le 24 \\ 1 - \dfrac{1}{15}\left(\dfrac{B_o}{t_o}\right) - 24 & \text{for } 24 < \dfrac{B_o}{t_o} \le 33 \\ 0.000062\left(\dfrac{B_o}{t_o}\right)^2 - 0.011225\left(\dfrac{B_o}{t_o}\right) + 0.705288 & \text{for } 33 < \dfrac{B_o}{t_o} \le 100 \end{cases} \quad (21)$$

For the sandwiched concrete, a value of 0.07 is used for the strain at the inflection point (ε_{ci}) as suggested by Ahmed et al. [25]. The equation proposed by Lim and Ozbakkaloglu [37] is utilized for the core-concrete, incorporating the column size effect by Ahmed et al. [25] as

$$\varepsilon_{ci} = 2.8\varepsilon_{cc}^{'}\left(\gamma_c f_c^{'}\right)^{-0.12}\left(\frac{f_{cr}}{f_{cc}^{'}}\right) + 10\varepsilon_{cc}^{'}\left(\gamma_c f_c^{'}\right)^{-0.47}\left(1 - \frac{f_{cr}}{f_{cc}^{'}}\right) \quad (22)$$

4.4. Tensile behavior of concrete

When subjected to eccentric loading, part of the concrete in a square CFDST slender column is in tension. The tensile stress-strain relationship of concrete is given in Fig. 7. The stress under tension increases linearly up to the tensile strength at which the concrete cracks and then linearly decreases to zero. The tensile strength of concrete is prescribed as $0.6\sqrt{\gamma_c f_c^{'}}$ in the numerical model and the ultimate tensile strain is equal to ten times the concrete cracking strain.

5. Comparisons of computational results with experimental data

In the absence of experimental data on CFDST slender columns with square sections under eccentric loading, test results on CFDST short columns provided by Qian et al. [18] and on

DCFST slender columns given by Han et al. [12] are used to validate the developed numerical model. Qian et al. [18] carried out experiments on eccentrically loaded short CFDST square columns with a length of 600 mm. The dimensions of the outer steel tubes were 180×180 mm with the thickness of either 3.62 mm or 5.40 mm. High strength concrete was used to construct these columns. The specimens were tested with the loading eccentricity varied from 18 to 54 mm. The cylindrical concrete strength $f_c^{'}$ was estimated by applying a reduction factor of 0.85 to the cube concrete strength as suggested by Oehlers and Bradford [41]. Table 1 gives the test data of the specimens tested by Qian et al. [18]. The predicted ultimate axial strengths using the mathematical model are found to be consistent with the test results tabulated in Table 1, in which $P_{u,num}$ and $P_{u,\exp}$ are the numerical and experimental ultimate axial loads of the columns, respectively. The mean $P_{u,num}/P_{u,\exp}$ ratio is 0.97. The predicted axial load-lateral displacement responses of CFDST columns are compared against experimental ones in Fig. 8 and Fig 9. In general, the computed axial load-lateral deflection curves are correlated well with corresponding test data. The small discrepancy between experimental and computational solutions is observed. It is likely caused by fact that the actual stiffness and strength of concrete in the tested specimens are unknown.

Table 2 presents the material as well as geometric properties of slender square double-skin concrete-filled steel tubes given by Han et al. [12]. The initial geometric imperfection of the columns was taken as $L/1000$ in the analyses. The measured ultimate loads of DCFST columns as well as predictions are also provided in Table 2. There is a good agreement between computed column strengths and measured values with a mean $P_{u,num}/P_{u,\exp}$ ratio of 0.96. The axial load-buckling displacement curves of DCFST columns are given in Fig. 10. The experimentally measured curves are generally captured well by the mathematical modeling procedure developed. However, the measured post-yield curves differ slightly from the computational

ones and the ductility of the test columns is slightly overestimated as the actual concrete strength and stiffness in tested columns are uncertain.

6. Local-global interaction buckling behavior

The mathematical model was implemented in a computer program, which was used to examine the influences of various factors on the interaction local-global buckling of CFDST square columns. The parameters investigated include the width-to-thickness ratio (B_o / t_o) of the external tube, the diameter-to-thickness ratio (D_i / t_i) of the internal tube, diameter-to-width ratio (D_i / B_o), column slenderness ratio (L / r), the loading eccentricity ratio (e / B_o), concrete strength ($f_c^{'}$), and steel yield strength (f_{sy}). The material and geometric properties of the reference column used in the parametric studies were: $B_o = 450$ mm, t_o =7.5 mm, D_i =150 mm, t_i =3.75 mm, $f_{syo} = f_{syi} = 350$ MPa, $E_s = 200$ GPa, $f_{co}^{'} = f_{ci}^{'} = 70$ MPa, e / B_o =0.3, *L/r*=50 and initial geometric imperfection = *L*/1000.

6.1. Influences of L/r ratio

Investigations on the influences of *L*/*r* ratio on the interaction local-global buckling responses of eccentrically loaded CFDST square columns were undertaken by means of altering the column length only. The calculated axial load-buckling displacement curves for the columns are plotted in Fig. 11. It would appear from Fig. 11 that the ultimate strength and initial stiffness of the CFDST columns decrease significantly as a result of increasing the *L*/*r* ratio. Figure 12 presents the column strength curve which is a function of the member slenderness ratio. When the column is short, its ultimate strength is reduced by only 5% by means of changing the *L/r*

ratio from 0.0 to 22. However, the ultimate load of the slender column represented as P_u in Fig. 12 incorporating an L/r ratio of 140 is 30% of the ultimate strength P_{oa}, which is the ultimate load of the eccentrically loaded column with the column slenderness ratio approaching zero.

6.2. Influences of B_o / t_o ratio

The sensitivities of the local-global interaction buckling strengths of CFDST columns to the B_o / t_o ratio were investigated by using the computer program. Changes were made only to the thickness of the external steel tube to produce the B_o / t_o ratios of 40, 60, 80 and 100, respectively. The column interaction responses of local-global buckling are provided in Fig. 13. The use of steel tube with a larger B_o / t_o ratio causes a remarkable reduction in the column ultimate load as well as its initial stiffness. The ultimate load of slender CFDST columns is reduced by 15.98%, 26.08% and 46.28%, respectively when increasing the B_o / t_o ratio from 40 to 60, 80 and 100. This is because increasing the B_o / t_o ratio induces a reduction in the cross-sectional area of the steel tubes that are susceptible to local buckling so that the column ultimate load decreases remarkably. The effect of B_o / t_o ratio on the column-strength-curves are demonstrated in Fig. 14, where P_{oa} is the ultimate load of the eccentrically loaded column with the B_o / t_o ratio of 40 and the column slenderness ratio approaching zero. It is noted that the column ultimate load decreases substantially when increasing the B_o / t_o ratio for same the member slenderness. The effect of the B_o / t_o ratio on the section axial strength is the most pronounced but increasing the column slenderness decreases its effect. When changing the B_o / t_o ratio from 40 to 60, 80 and 100, the section axial load reduces by 14%, 22.5% and 39.8%, respectively.

6.3. Influences of D_i / B_o ratio

The computer program developed was utilized to study the responses of loaded CFDST slender columns to the changes of D_i / B_o ratios. The diameter of the inner circular tube was altered from 150 mm to 200 mm, 250 mm and 300 mm. The D_i / B_o ratios of these sections were calculated as 0.33, 0.44, 0.55 and 0.66, respectively. Figure 15 presents the computed axial load-buckling displacement curves which are dependent on the D_i / B_o ratio. It is shown that the D_i / B_o ratio has only a minor influence on the column overall buckling behavior. The effect of D_i / B_o ratio on the strength curves for columns is illustrated in Fig. 16, where P_{oa} is the ultimate load of the eccentrically loaded column with the D_i / B_o ratio of 0.33 and the column slenderness ratio approaching zero. The effect of D_i / B_o ratio is also insignificant. When the D_i / B_o ratio is changed from 0.33 to 0.66, the section axial load reduces by 5% while its column strength with L / r =140 reduces only 4.5%.

6.4. Influences of e / B_o ratio

The investigation into the sensitivities of the interaction local-global buckling behavior of CFDST columns to the loading eccentricity ratio (e / B_o) was conducted by using the proposed computational model. The e / B_o ratios of 0.2, 0.25, 0.3 and 0.35 were considered in the investigation. It is seen from Fig. 17 that as a result of using a larger e / B_o ratio, a sustainable reduction in the column initial stiffness as well as its ultimate load is obtained. This is attributed to the increase in the second order effects of the column. The column ultimate strength is reduced by 35.3% by changing the e / B_o ratio from 0.2 to 0.35. The influences of e / B_o ratio

on the ultimate strength of CFDST slender columns are illustrated in Fig. 18, where P_{oa} is the ultimate load of the concentrically loaded slender column. Increasing e / B_o ratio remarkably reduces the ultimate strength of the column. Figure 19 gives the column strength curves of square CFDST columns with varying e / B_o ratios, in which P_{oa} is taken as the ultimate load of the eccentrically loaded column with the e / B_o ratio of 0.2 and the column slenderness ratio approaching zero. It is evident that increasing the e / B_o ratio decreases the column ultimate strength regardless of the member slenderness.

6.5. Influences of D_i / t_i ratio

The influences of D_i / t_i ratio on the behavior of slender CFDST columns were examined by varying the D_i / t_i ratio from 20 to 50. The internal tube thickness was varied while the other parameters were unchanged. The local-global interaction buckling behavior of the slender columns is illustrated in Fig. 20. It is discovered that the complete curves of axial load-buckling displacement for the slender CFDST columns are not sensitive to the D_i / t_i ratio. The post-peak load-buckling displacement curves cannot be distinguished for different D_i / t_i ratios. By increasing D_i / t_i ratio from 20 to 50, the column ultimate load decreases by 1.25% only. The reason for this is that the global buckling of square CFDST slender columns mainly depends on the B_o / t_o ratio, member slenderness and e / B_o ratios. The column strength curves of square CFDST beam-columns with varying D_i / t_i ratios are given in Fig. 21, in which P_{oa} is the ultimate load of the eccentrically loaded column with the D_i / t_i ratio of 20 and the column slenderness ratio approaching zero. It is obvious from Fig. 21 that D_i / t_i ratio has an insignificant effect on the column strength curves.

6.6. Influences of local buckling

The influence of the outward local-buckling of the outer tubes with square sections on the global buckling of CFDST slender columns under eccentric loading was investigated. The B_o / t_o and e / B_o ratios of the column were taken as 100 and of 0.5, respectively. As demonstrated in Fig. 22, the columns ultimate load is overestimated by 8.4% when the analysis ignored local buckling. The sensitivities of the column strength curve to the local buckling of the square section are shown in Fig. 23, in which P_{oa} is the ultimate load of the eccentrically loaded column with the column slenderness ratio approaching zero considering local buckling. Local buckling has the most prominent influence on the section axial-load capacity. However, its effect on the column strength decreases when the column slenderness increases. For very slender CFDST columns with a L / r ratio greater than 200, the local buckling effect diminishes. This is because the ultimate strength of very slender columns is mainly governed by the global buckling and the strength reduction due to the local buckling can be ignored.

6.7. Influences of concrete strength

The concrete in square CFDST slender columns carries most of the compressive load. It is vital to understand the influences of high-strength concrete on the interaction local-global buckling responses of slender CFDST columns for the economical design of such columns. Three different scenarios were considered as follows: (1) the sandwiched-concrete and core-concrete had the same compressive strength; (2) the sandwiched-concrete strength was varied from 40 MPa to 70 MPa while the core-concrete strength was not changed; and (3) the sandwiched-concrete strength was not changed while the core-concrete strength was varied from 40 MPa to 70 MPa. For the first case, the axial load-buckling displacement curves of CFDST columns

with different concrete strengths are given in Fig. 24. The column ultimate load is increased by 10.0%, 17.8% and 23.9%, respectively, by changing the concrete strength from 40 MPa to 50, 60 and 70 MPa. The column strength curves which are dependent on the concrete strengths are provided in Fig. 25, in which P_{oa} is the ultimate load of the eccentrically loaded column with $f_c^{'} = 40$ MPa and the column slenderness ratio approaching zero. The use of higher strength concrete leads to a higher column ultimate load irrespective of its slenderness ratio. However, the concrete strength effect decreases as the column slenderness increases. When changing the concrete strength from 40 MPa to 70 MPa, the section axial capacity increases by 36% while its member axial strength with L / r =140 increases by 13.5%. The influences of sandwiched-concrete strength on the load-deflection curves and column strength curves are illustrated in Fig. 26 and Fig. 27, respectively. In Fig. 27, P_{oa} is the ultimate load of the eccentrically loaded column with $f_{co}^{'} = 40$ MPa and the column slenderness ratio approaching zero. The effects of the core-concrete strength on the structural behavior are presented in Fig. 28 and Fig. 29, in which P_{oa} is the ultimate load of the eccentrically loaded column with $f_{ci}^{'} = 40$ MPa and the column slenderness ratio approaching zero. It can be seen that the sandwiched-concrete strength has a remarkable effect on the global buckling behavior of square slender CFDST columns but the influence of core-concrete strength is insignificant.

6.8. Influences of steel yield strength

The studies on the inelastic buckling behavior of slender square CFDST columns with various steel yield strengths were undertaken. Three cases were investigated. The first case was to change the yield stress of both external and inner steel tubes from 350 MPa to 450 MPa, 550 MPa, and 650 MPa. The interaction local-global buckling responses of CFDST columns that are a function of the steel yield stress are given in Fig. 30. The figure shows that the yield stress

of both tubes does not affect the column initial stiffness, but remarkably increases the column axial capacity. As shown in Fig. 30, when the steel yield stress of the tubes is changed from 350 MPa to 650 MPa, the percentage increase in the column ultimate strength with a L/r ratio of 40 is 20.8%. The influences of steel yield strength on the column strength curves are shown in Fig. 31, in which P_{oa} is the ultimate load of the eccentrically loaded column with $f_{sy} = 350$ MPa and the column slenderness ratio approaching zero. The effect of the steel yield stress of both tubes on the column ultimate load decreases as the L/r ratio increases. The second case was to alter only the yield strength of the internal steel tube. As depicted in Figs. 32 and 33, the effect of internal steel tube yield stress on the load-buckling displacement responses and column strength curves is very minor and can be ignored. In Fig. 33, P_{oa} is the ultimate load of the eccentrically loaded column with $f_{syi} = 350$ MPa and the column slenderness ratio approaching zero. The third case was to vary the yield strength of the external steel tube only. It is seen from Figs. 34 and 35 that the global buckling responses and the column strength curves are affected predominantly by the yield strength of the external steel tube. In Fig. 35, P_{oa} is the ultimate load of the eccentrically loaded column with $f_{syo} = 350$ MPa and the column slenderness ratio approaching zero. Thus, it is effective to use high strength external steel tube to improve the strength of CFDST columns with short and immediate lengths.

7. Proposed design models

7.1. CFDST slender columns under axial compression

The computational model developed in this study has been used to obtain the column strength curves for square CFDST columns under axial compression with a wide range of parameters and initial geometric imperfection of $L/1000$. Based on the numerical results and Eurocode 4

[42], a simple design model for calculating the ultimate strength of square slender CFDST columns loaded concentrically is proposed herein as:

$$P_{u,des} = \chi P_{uo} \tag{23}$$

where P_{uo} is the column section ultimate strength under axial compression and calculated as

$$P_{uo} = f_{syo}A_{soe} + f_{syi}A_{si} + \gamma_{co} f_{co}^{'} A_{co} + \gamma_{ci} f_{ci}^{'} A_{ci} \tag{24}$$

where A_{soe} is the effective area of the outer tube conserving local buckling effects, A_{si} the cross-sectional area of inner tube, A_{co} the cross-sectional area of sandwiched concrete, A_{ci} the cross-sectional area of core concrete, $f_{co}^{'}$ and $f_{ci}^{'}$ the compressive strength of sandwiched-concrete and core-concrete, respectively.

In Eq. (23), χ is the slenderness reduction factor. The original expression for χ suggested by Eurocode 4 is modified herein as:

$$\chi = \frac{1}{\varphi + \sqrt{\varphi^2 - \overline{\lambda}^2}} \leq 1.0 \tag{25}$$

$$\varphi = \frac{1.03 + 0.21(\overline{\lambda} - 0.2) + \overline{\lambda}^2}{2} \tag{26}$$

The relative slenderness ratio $\overline{\lambda}$ is expressed as

$$\bar{\lambda} = \sqrt{\frac{P_{uo}}{P_{cr}}} \tag{27}$$

in which P_{cr} is the Euler buckling load of CFDST columns and computed by

$$P_{cr} = \frac{\pi^2 (EI)_{eff}}{L^2} \tag{28}$$

in which $(EI)_{eff}$ is the effective flexural stiffness of the composite cross-section, expressed as

$$(EI)_{eff} = E_{s,so} I_{s,so} + 0.6 E_{cm,co} I_{c,co} + E_{s,si} I_{s,si} + 0.6 E_{cm,ci} I_{c,ci} \tag{29}$$

where E_s is the Young's modulus of steel, I_s the second moment of area of the steel tube, E_{cm} the Young's modulus of concrete, I_c the second moment of area of concrete. The subscripts *so*, *si*, *co* and *ci* define the outer steel tube, inner steel tube, sandwiched concrete and core concrete, respectively. The Young's modulus of concrete can be estimated by

$$E_{cm} = 22000 \left(\frac{f_c^{'} + 8}{10} \right)^{1/3} \tag{30}$$

Figure 36 presents the validation of the proposed design model. The column strength curve of the reference column given in Section 6 is compared with the one calculated using the design model. It is shown that the agreement between numerical predictions and design calculations is good. Therefore, the proposed design model can be used in the design of square CFDST slender columns loaded concentrically in practice.

7.2. CFDST slender columns under eccentric loading

The numerical models developed by Liang et al. [24] and in this paper were employed to generate the axial load-moment interaction diagrams of square CFDST slender columns considering local buckling. Based on the numerical studies, the nominal interaction equations for CFDST slender columns with non-compact or slender sections under eccentric loading are proposed as

$$M_u = 1.04M_o\left[1-\left(\frac{P_u}{P_o}\right)^{\alpha_m}\right] \qquad \text{for } P_u \geq 0.2P_o \tag{31}$$

$$M_u = M_o\left[1-\frac{1}{10}\left(\frac{P_u}{P_o}\right)^{\alpha_n}\right] \qquad \text{for } P_u < 0.2P_o \tag{32}$$

where P_u is the axial load, M_u the corresponding ultimate bending resistance of the slender CFDST column, P_o the ultimate axial strength of the slender column without moment, M_o the column ultimate bending resistance without axial load, α_m and α_n the shape factors of the interaction curves depending on the *L/r* ratio of CFDST columns and are proposed as

$$\alpha_m = 2.44 - 0.012\left(\frac{L}{r}\right) \qquad (1.0 \leq \alpha_m \leq 2.0) \tag{33}$$

$$\alpha_n = \begin{cases} 2.668\left(L/r\right) - 2.496 & \text{for } 1.0 \leq \alpha_m \leq 1.5 \\ 1.5 & \text{for } 1.5 < \alpha_m \leq 2.0 \end{cases} \tag{34}$$

The comparison of the interaction curves for CFDST columns with various design parameters given in the parametric study obtained by the proposed equations and the numerical model is

shown in Fig. 37. It is seen that the agreement between the proposed design equations and numerical results for a wide range of design parameters is good. The design interaction curves are also compared with those computed by the formulas given in AISC 360-16 [43]. The proposed design equations yield better results than those specified in AISC 360-16 as can be seen from Fig. 37.

8. Conclusions

This paper has reported on the development of a mathematical model incorporating the fiber approach for the simulation of the interaction local-global buckling responses of slender CFDST beam-columns with thin-walled square sections loaded eccentrically. Salient features associated with slender CFST square columns have been taken into consideration in the formulation of the mathematical model, including confinement, local-global interaction buckling, geometric imperfection, and second-order as well as high-strength materials. Efficient computational solution algorithms implementing the inverse quadratic method have been developed to obtain converged solutions to the nonlinear dynamic functions generated in the incremental-iterative analysis process for slender CFDST columns. The computational model has been verified by test data on CFDST and DCFST columns and employed to determine the local-global interaction buckling behavior of CFDST columns with various important parameters. Design models have been developed for calculating the ultimate strengths of slender square CFDST columns subjected to axial compression and eccentric loading.

The concluding remarks are provided as follows:

(1) Further tests on the behavior of slender square CFDST columns should be conducted to provide results that can be used to validate numerical models.

(2) The initial stiffness and ultimate axial load of square CFDST columns are found to reduce significantly when increasing the column slenderness ratio.

(3) The B_o / t_o ratio has a remarkable effect on the strength and initial stiffness of CFDST columns but its influence decreases with increasing the column slenderness.

(4) The D_i / B_o ratio has a minor influence on the global buckling behavior of CFDST columns.

(5) Increasing the e / B_o ratio results in marked reductions in the column initial stiffness and ultimate axial load.

(6) The buckling behavior of slender CFDST columns is almost not affected by the D_i / t_i ratio.

(7) The outward local buckling of the outer steel tube considerably reduces the ultimate load of CFDST square columns, but this effect decreases when the column slenderness increases.

(8) Increasing the sandwiched-concrete strength substantially improves the column ultimate load. The influence of concrete strength, however, decreases with increasing the column slenderness ratio. The core-concrete strength has an insignificant influence on the column strength.

(9) The ultimate strength of CFDST columns is shown to increase appreciably by using higher yield strength external steel tube. However, the column global buckling behavior is almost not affected by the yield stress of the inner steel Tube.

(10) The proposed design models derived based on the numerical results predict well the ultimate strengths of square CFDST slender columns under axial compression and eccentric loading.

References

[1] AS 3600-2009, Australian Standard for Concrete structures, Standards Australia, Sydney, NSW, Australia, 2009.

[2] A.H. Varma, J.M. Ricles, R. Sause, and L.W. Lu, Experimental behavior of high strength square concrete-filled steel tube beam-columns, J. Struc. Eng. ASCE 128 (3) (2002) 309-318.

[3] M. Mursi and B. Uy, Strength of concrete filled steel box columns incorporating interaction buckling, J. Struc. Eng. ASCE 129 (5) (2003) 626-639.

[4] M. Mursi and B. Uy, Strength of slender concrete filled high strength steel box columns, J. Constr. Steel Res. 60 (12) (2004) 1825-1848.

[5] D. Liu, Behaviour of high strength rectangular concrete-filled steel hollow section columns under eccentric loading, Thin-Walled Struct. 42 (12) (2004) 1631-1644.

[6] Y. Du, Z. Chen, Y B. Wang, and J.Y.R. Liew, Ultimate resistance behavior of rectangular concrete-filled tubular beam-columns made of high-strength steel, J. Constr. Steel Res. 133 (2017) 418-433.

[7] Y. Du, Z. Chen, J.Y.R. Liew, and M.X. Xiong, Rectangular concrete-filled steel tubular beam-columns using high-strength steel: Experiments and design, J. Constr. Steel Res. 131 (2017) 1-18.

[8] Z. Tao and L.H. Han, Behaviour of concrete-filled double skin rectangular steel tubular beam–columns, J. Constr. Steel Res. 62 (7) (2006) 631-646.

[9] Z. Tao, L.H. Han, and X.L. Zhao, Behaviour of concrete-filled double skin (CHS inner and CHS outer) steel tubular stub columns and beam-columns, J. Constr. Steel Res. 60 (8) (2004) 1129-1158.

[10] X L. Zhao, R. Grzebieta, and M. Elchalakani, Tests of concrete-filled double skin CHS composite stub columns, Steel and Composite Structures 2 (2) (2002) 129-146.

[11] X.L. Zhao, L.W. Tong, and X.Y. Wang, CFDST stub columns subjected to large deformation axial loading, Eng. Struct. 32 (3) (2010) 692-703.

[12] L.H. Han, Z. Tao, H. Huang, and X.L. Zhao, Concrete-filled double skin (SHS outer and CHS inner) steel tubular beam-columns, Thin-Walled Struct. 42 (9) (2004) 1329-1355.

[13] L.H. Han, H. Huang, Z. Tao, and X.L. Zhao, Concrete-filled double skin steel tubular (CFDST) beam–columns subjected to cyclic bending, Eng. Struct. 28 (12) (2006) 1698-1714.

[14] M.X. Xiong, D.X. Xiong, and J.Y.R. Liew, Behaviour of steel tubular members infilled with ultra high strength concrete, J. Constr. Steel Res. 138 (2017) 168-183.

[15] W.J. Pei, Research on Mechanical Performance of Multibarrel Tube-Confined Concrete Columns, ME Thesis, Chang'an Univ., Xian, China, 2005 (in Chinese).

[16] J. Qian, N. Li, X. Ji, and Z. Zhao, Experimental study on the seismic behavior of high strength concrete filled double-tube columns, Earthq. Eng. Eng. Vib. 13 (1) (2014) 47-57 (in Chinese).

[17] J. Qian, Y. Zhang, X. Ji, and W. Cao, Test and analysis of axial compressive behavior of short composite-sectioned high strength concrete filled steel tubular columns, J. Build. Struct. 32 (12) (2011) 162-169 (in Chinese).

[18] J. Qian, Y. Zhang, and W. Zhang, Eccentric compressive behavior of high strength concrete filled double-tube short columns, J. Tsinghua Univ. 55 (1) (2015) 1-7 (in Chinese).

[19] M.X. Xiong, D.X. Xiong, and J.Y.R. Liew, Axial performance of short concrete filled steel tubes with high-and ultra-high-strength materials, Eng. Struct. 136 (2017) 494-510.

[20] Z.B. Wang, Z. Tao, and Q. Yu, Axial compressive behaviour of concrete-filled double-tube stub columns with stiffeners, Thin-Walled Struct. 120 (2017) 91-104.

[21] N.E. Shanmugam, B. Lakshmi, and B. Uy, An analytical model for thin-walled steel box columns with concrete in-fill, Eng. Struct. 24 (6) (2002) 825-838.

[22] Z. Vrcelj and B. Uy, Strength of slender concrete-filled steel box columns incorporating local buckling, J. Constr. Steel Res. 58 (2) (2002) 275-300.

[23] V.I. Patel, Q.Q. Liang, and M.N.S. Hadi, High strength thin-walled rectangular concrete-filled steel tubular slender beam-columns, Part I: Modeling, J. Constr. Steel Res. 70 (2012) 377-384.

[24] Q.Q. Liang, V.I. Patel, and M.N.S. Hadi, Biaxially loaded high-strength concrete-filled steel tubular slender beam-columns, Part I: Multiscale simulation, J. Constr. Steel Res. 75 (2012) 64-71.

[25] M. Ahmed, Q.Q. Liang, V.I.Patel, and M.N.S. Hadi, Nonlinear analysis of rectangular concrete-filled double steel tubular short columns incorporating local buckling, Eng. Struct. 175 (2018) 13-26.

[26] T.Q. Lü and G.F. Zhao, Numerical method for analysis of ultimate strength of concrete-filled square steel Tubular columns under eccentric compression reinforced by inner circular steel tube, J. Dalian Univ. Techn. 41 (5) (2001) 612-616 (in Chinese).

[27] Q.Q. Liang, Performance-based analysis of concrete-filled steel tubular beam–columns, Part I: Theory and algorithms, J. Constr. Steel Res. 65 (2) (2009) 363-372.

[28] Q.Q. Liang, Performance-based analysis of concrete-filled steel tubular beam–columns, Part II: Verification and applications, J. Constr. Steel Res. 65 (2) (2009) 351-362.

[29] Q.Q. Liang, Analysis and Design of Steel and Composite Structures, CRC Press, Taylor and Francis Group, Boca Raton and London, 2014.

[30] V.I. Patel, Q.Q. Liang, and M.N.S. Hadi, Concrete-Filled Stainless Steel Tubular Columns, CRC Press, Taylor and Francis, Boca Raton and London, 2018.

[31] P.O. Persson and G. Strang, A simple mesh generator in MATLAB, SIAM Rev. 46 (2) (2004) 329-345.

[32] M. Ahmed, Q.Q. Liang, V.I. Patel, and M.N.S. Hadi, Numerical analysis of axially loaded circular high strength concrete-filled double steel tubular short columns, Thin-Walled Struct. 138 (2019) 105-116.

[33] Q.Q. Liang, B. Uy, and J.Y.R. Liew, Local buckling of steel plates in concrete-filled thin-walled steel tubular beam–columns, J. Constr. Steel Res. 63 (3) (2007) 396-405.

[34] Q.Q. Liang, High strength circular concrete-filled steel tubular slender beam–columns, Part I: Numerical analysis, J. Constr. Steel Res. 67 (2) (2011) 164-171.

[35] J.B. Mander. Seismic design of bridge piers (Ph.D. Thesis), Depart. of Civil Eng. Uni. of Canterbury, Christchurch, New Zealand, 1983..

[36] J.B. Mander, M.J. Priestley, and R. Park, Theoretical stress-strain model for confined concrete, J. Struc. Eng. ASCE 114 (8) (1988) 1804-1826.

[37] J.C. Lim and T. Ozbakkaloglu, Stress–strain model for normal-and light-weight concretes under uniaxial and triaxial compression, Constr. Build. Mater. 71 (2014) 492-509.

[38] Q.Q. Liang and S. Fragomeni, Nonlinear analysis of circular concrete-filled steel tubular short columns under axial loading, J. Constr. Steel Res. 65 (12) (2009) 2186-2196.

[39] H.T. Hu, C.S. Huang, M.H. Wu, and Y.M. Wu, Nonlinear analysis of axially loaded concrete-filled tube columns with confinement effect, J. Struc. Eng. ASCE 129 (10) (2003) 1322-1329.

[40] J. Tang, S. Hino, I. Kuroda, and T. Ohta, Modeling of stress-strain relationships for steel and concrete in concrete filled circular steel tubular columns, Steel Constr. Eng. JSSC 3 (11) (1996) 35-46.

[41] D.J. Oehlers and M.A. Bradford, Elementary Behaviour of Composite Steel and Concrete Structural Members, Butterworth-Heinemann, Oxford U.K., 1999.

[42] Eurocode 4, Design of Composite Steel and Concrete Structures-Part 1-1: General Rules and Rules for Buildings, European Committee for Standardization, CEN, Brussels, Belgium. EN 1994-1-1, 2004.

[43] AISC 360-16, Specification for Structural Steel Buildings. American Institute of Steel Construction, Chicago (IL), 2016.

Figures and tables

Table 1. Comparison of predicted and experimental ultimate axial loads of square CFDST beam-columns

Specimen	Outer Tube			Inner Tube			Concrete		e (mm)	Ultimate load			Ref.
	$B_o \times B_o \times t_o$ (mm)	$\frac{B_o}{t_o}$	f_{syo} (MPa)	$D_i \times t_i$ (mm)	$\frac{D_i}{t_i}$	f_{syi} (MPa)	f'_{co} (MPa)	f'_{ci} (MPa)		$P_{u,\exp}$ (kN)	$P_{u,num}$ (kN)	$\frac{P_{u,num}}{P_{u,\exp}}$	
I-CFDT1-1	180×180×3.62	49.7	348	89×2.6	34.2	314	89.85	74.38	18	2690	2585	0.96	[18]
I-CFDT3-1	180×180×3.62	49.7	348	114×3.35	34.0	328	89.85	74.38	18	2712	2746	1.01	
I-CFDT3-2	180×180×3.62	49.7	348	114×3.35	34.0	328	89.85	74.38	36	2177	2200	1.01	
I-CFDT3-3	180×180×3.62	49.7	348	114×3.35	34.0	328	89.85	74.38	54	1927	1801	0.93	
I-CFDT5-1	180×180×3.62	49.7	348	140×2.84	49.3	345	89.85	74.38	45	1933	1982	1.03	
I-CFDT7-1	180×180×5.40	33.3	338	89×2.6	34.2	314	89.85	74.38	18	3127	2879	0.92	
I-CFDT9-1	180×180×5.40	33.3	338	114×3.35	34.0	328	89.85	74.38	18	3186	3237	1.02	
I-CFDT9-2	180×180×5.40	33.3	338	114×3.35	34.0	328	89.85	74.38	36	2474	2388	0.97	
I-CFDT9-3	180×180×5.40	33.3	338	114×3.35	34.0	328	89.85	74.38	27	2897	2640	0.91	
I-CFDT11-1	180×180×5.40	33.3	338	140×2.84	49.3	345	89.85	74.38	27	2752	2605	0.95	
II-CFDT3-1	180×180×3.62	49.7	348	114×3.35	34.0	328	74.38	89.85	18	2624	2591	0.99	
II-CFDT3-2	180×180×3.62	49.7	348	114×3.35	34.0	328	74.38	89.85	36	2087	2112	1.01	
II-CFDT3-3	180×180×3.62	49.7	348	114×3.35	34.0	328	74.38	89.85	54	1797	1715	0.95	
III-CFDT3-1	180×180×3.62	49.7	348	114×3.35	34.0	328	74.38	74.38	18	2623	2495	0.95	
III-CFDT3-2	180×180×3.62	49.7	348	114×3.35	34.0	328	74.38	74.38	36	2123	2042	0.96	
III-CFDT3-3	180×180×3.62	49.7	348	114×3.35	34.0	328	74.38	74.38	54	1740	1670	0.96	
Mean												0.97	
Standard Deviation (SD)												0.04	
Coefficients of Variance (COV)												0.04	

Table 2. Comparison of predicted and experimental ultimate axial loads of square DCFST slender beam-columns

Specimen	L (mm)	Outer tube			Inner tube			Concrete	e (mm)	Ultimate load			Ref.
		$B_o \times B_o \times t_o$ (mm)	$\frac{B_o}{t_o}$	f_{syo} (MPa)	$D_i \times t_i$ (mm)	$\frac{D_i}{t_i}$	f_{syi} (MPa)	f'_{co} (MPa)		$P_{u,\exp}$ (kN)	$P_{u,num}$ (kN)	$\frac{P_{u,num}}{P_{u,\exp}}$	
scbc1-1	1070	120×120×3	40	275.9	58×3	19.3	374.5	39.78	4	856	863	1.01	[12]
scbc1-2	1070	120×120×3	40	275.9	58x3	19.3	374.5	39.78	4	872	863	0.99	
scbc2-1	1070	120×120×3	40	275.9	58×3	19.3	374.5	39.78	14	667	704	1.06	
scbc2-2	1070	120×120×3	40	275.9	58x3	19.3	374.5	39.78	14	750	704	0.94	
scbc3-1	1070	120×120×3	40	275.9	58×3	19.3	374.5	39.78	45	480	438	0.91	
scbc3-2	1070	120×120×3	40	275.9	58x3	19.3	374.5	39.78	45	486	438	0.90	
scbc5-1	2136	120×120×3	40	275.9	58×3	19.3	374.5	39.78	15.5	596	555	0.93	
scbc5-2	2136	120×120×3	40	275.9	58x3	19.3	374.5	39.78	15.5	570	555	0.97	
scbc6-1	2136	120×120×3	40	275.9	58×3	19.3	374.5	39.78	45	380	354	0.93	
scbc6-2	2136	120×120×3	40	275.9	58x3	19.3	374.5	39.78	45	379	354	0.93	
Mean												0.96	
Standard Deviation (SD)												0.05	
Coefficients of Variance (COV)												0.05	

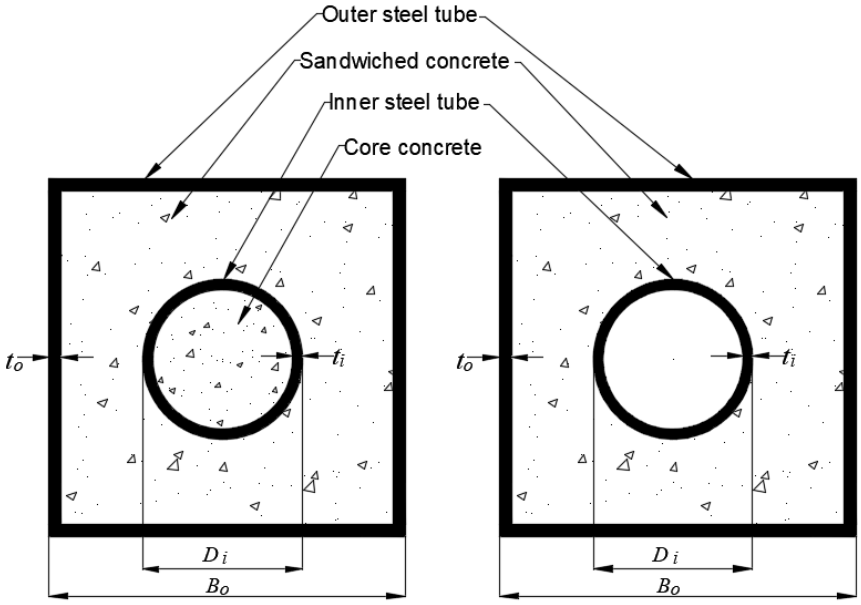

(a) (b)

Fig. 1. Cross-section of square concrete-filled steel tubular columns: (a) CFDST column; (b) DCFST column.

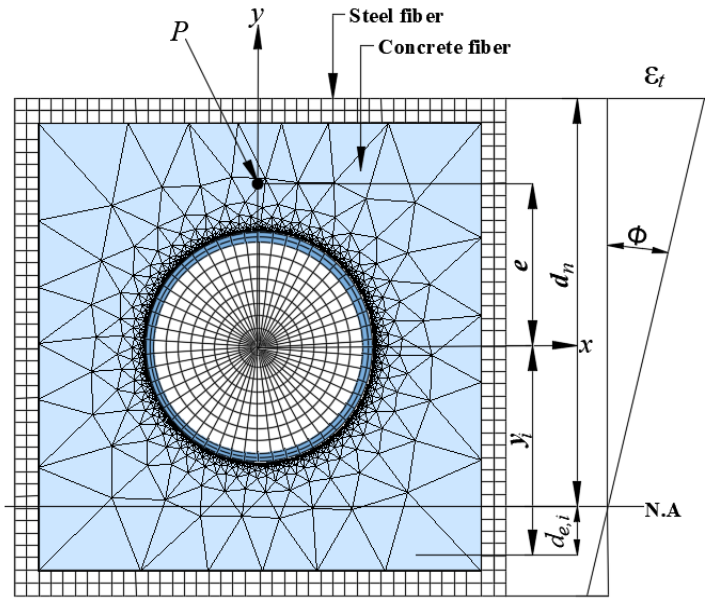

Fig. 2. Discretization and strain distribution of square CFDST column.

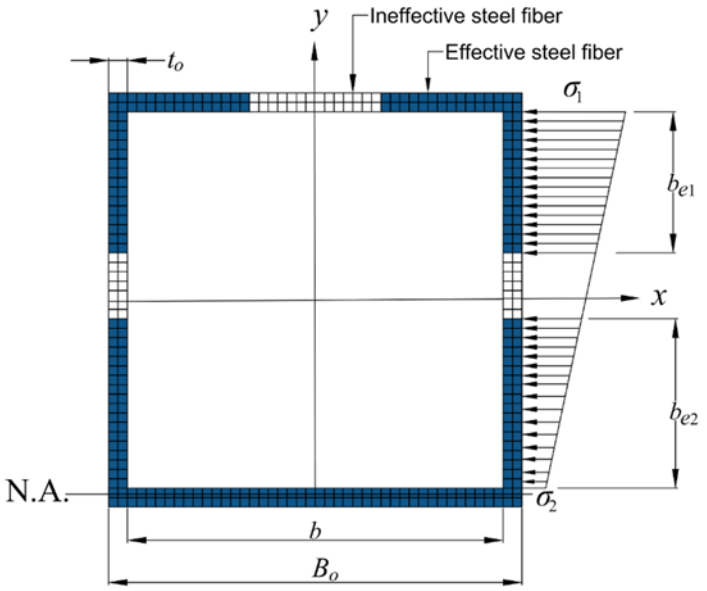

Fig. 3. Effective width of the external steel tube of square CFDST column.

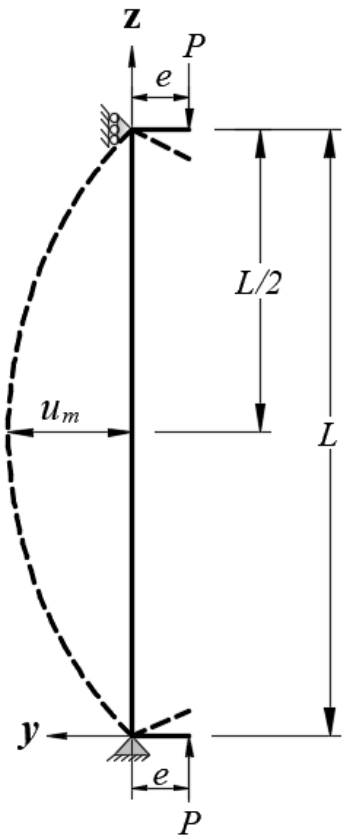

Fig. 4. Pin-ended CFDST slender beam-column.

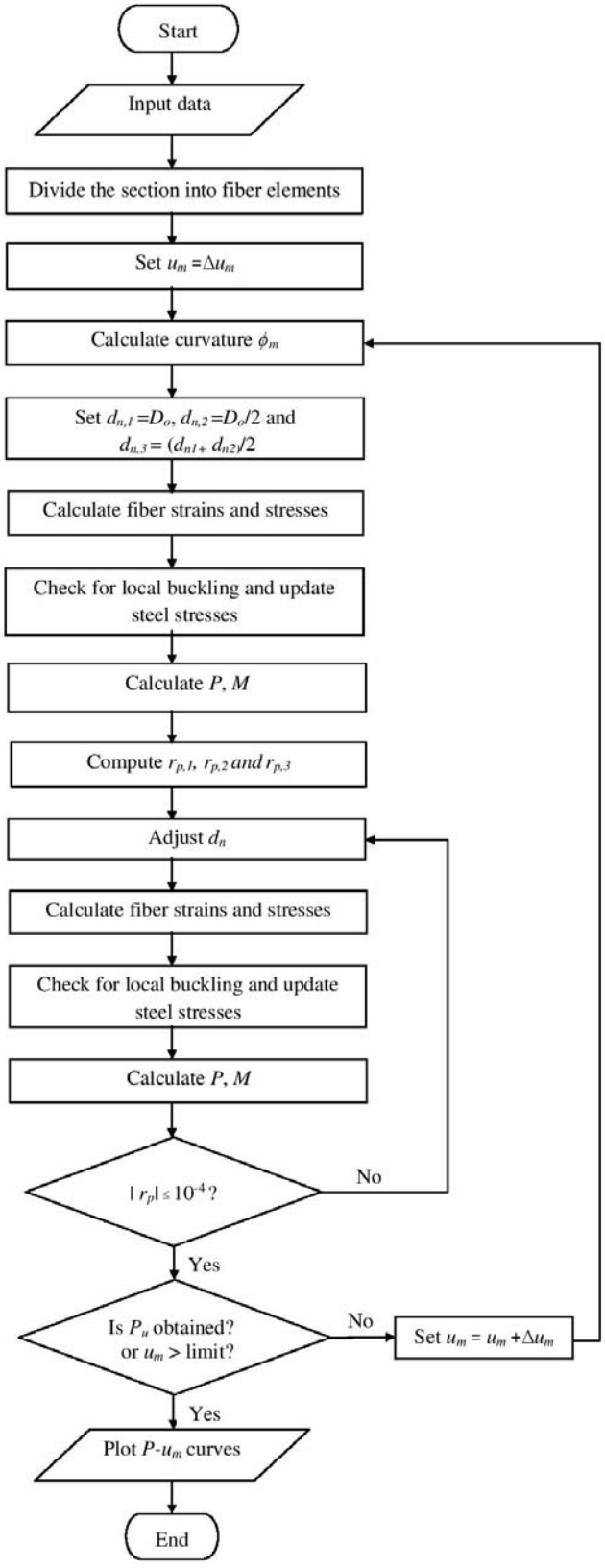

Fig. 5. Computer flowchart for calculating the axial load-deflection curves of square CFDST slender beam-columns.

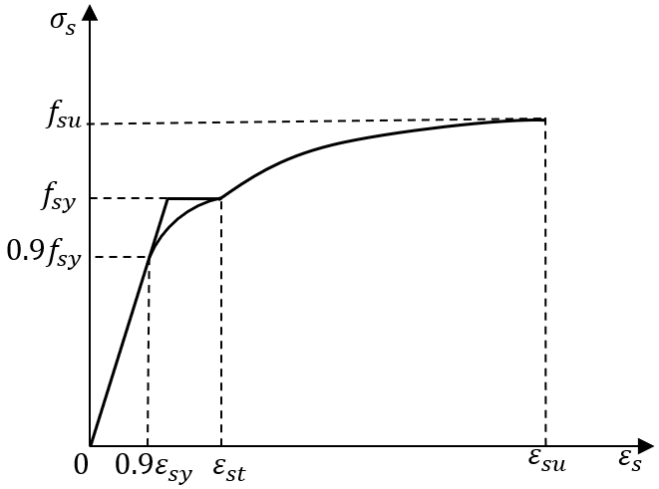

Fig. 6. Stress-strain curve for structural steels.

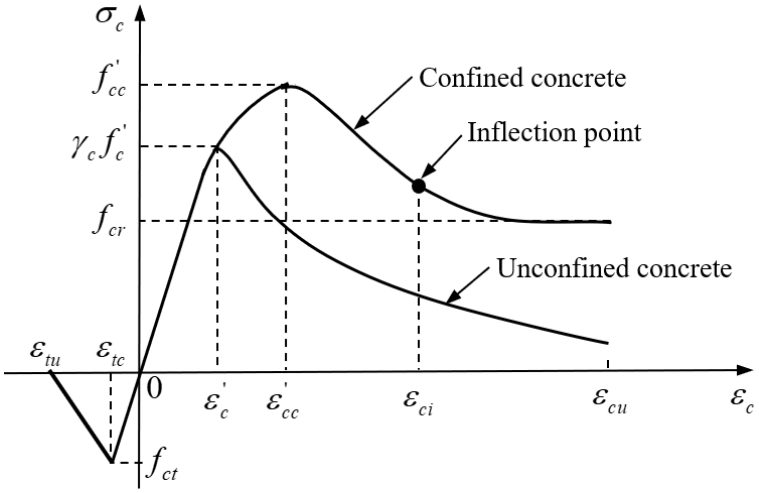

Fig. 7. Stress-strain curves for confined and unconfined concrete.

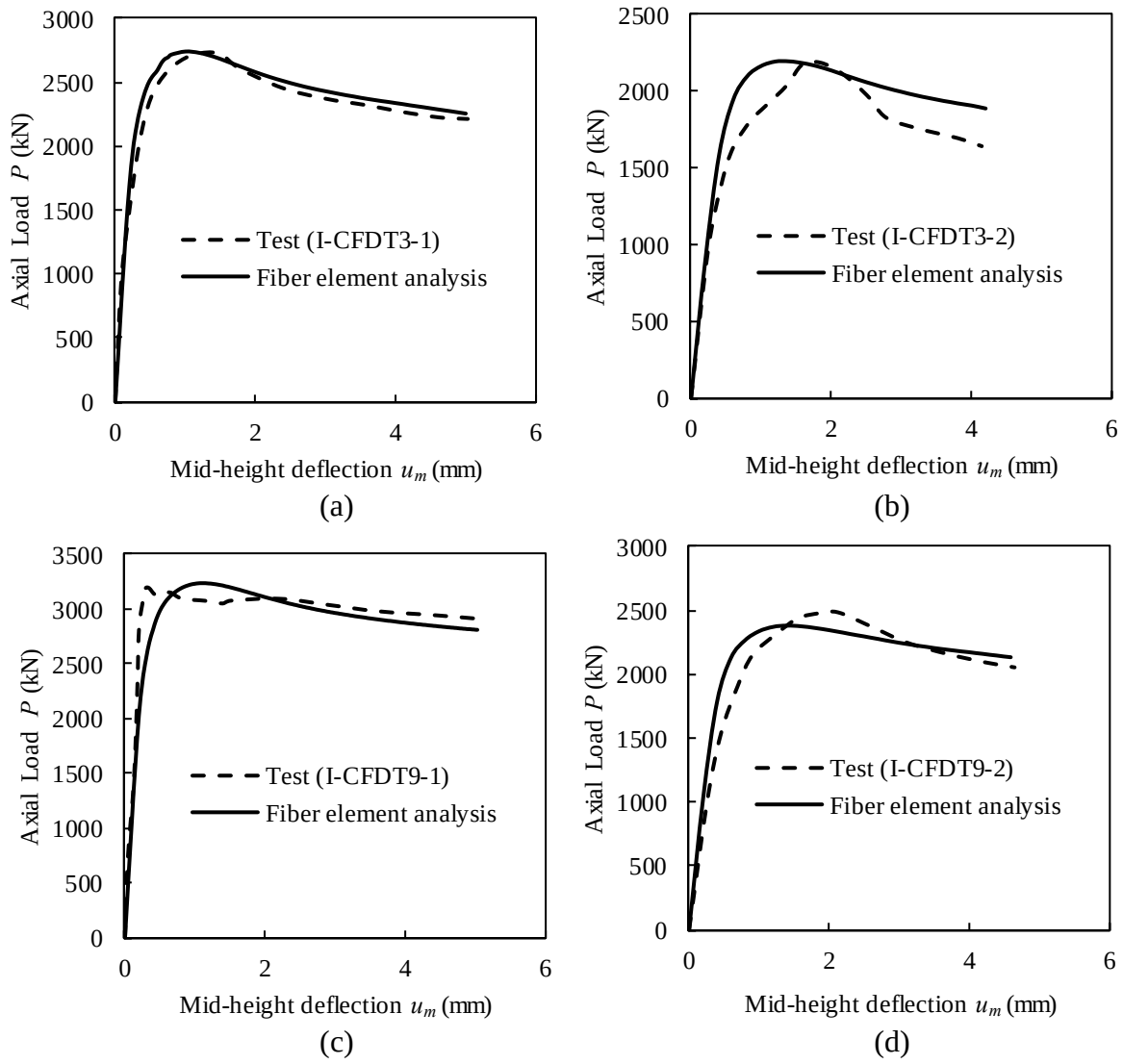

Fig. 8. Comparison of predicted and experimental axial load-deflection curves of square CFDST beam-columns tested by Qian et al. [18].

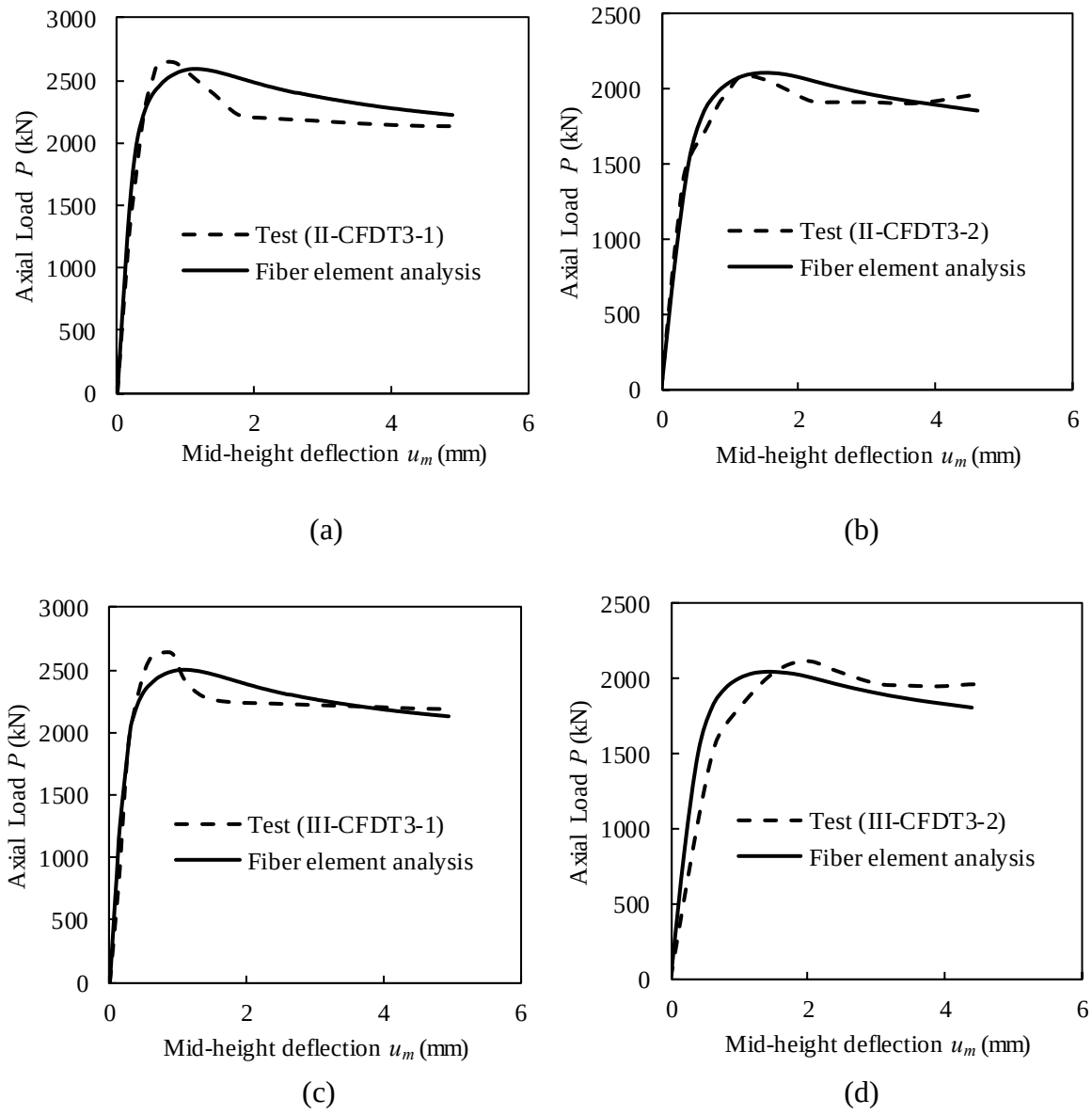

Fig. 9. Comparison of predicted and experimental axial load-deflection curves of square CFDST beam-columns tested by Qian et al. [18].

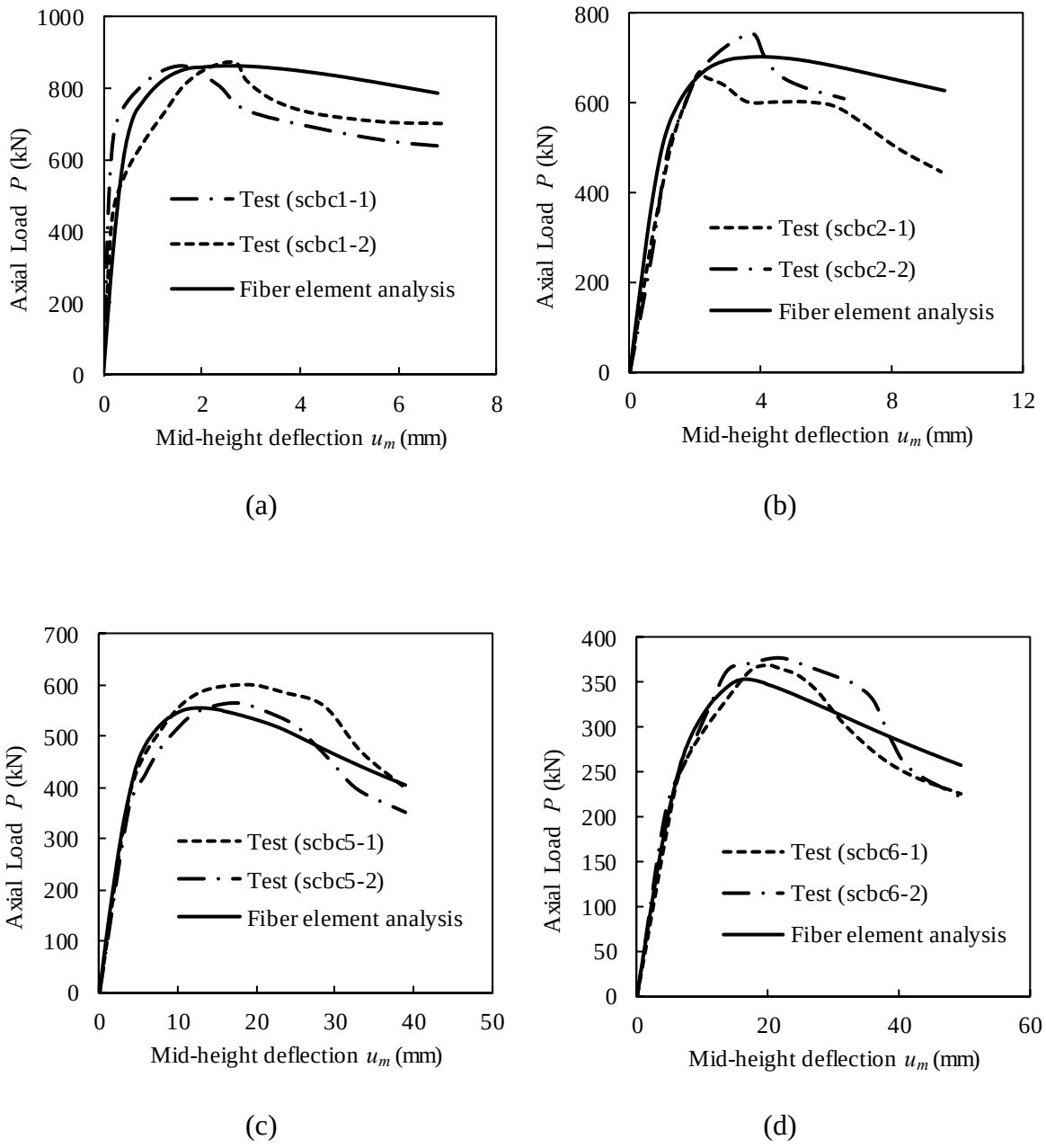

Fig. 10. Comparison of predicted and experimental axial load-deflection curves of square DCFST slender beam-columns tested by Han et al. [12].

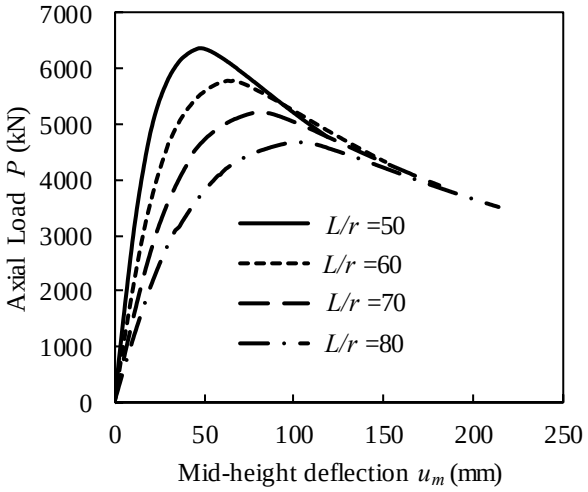

Fig. 11. Influences of L/r ratio on the axial load-deflection curves of square CFDST slender columns.

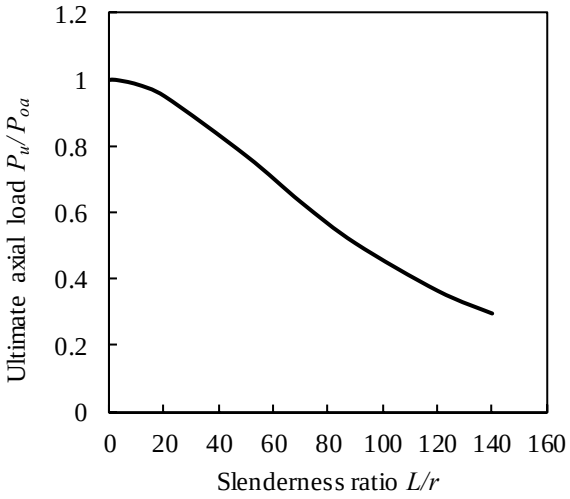

Fig. 12. The column strength curve of square CFDST columns.

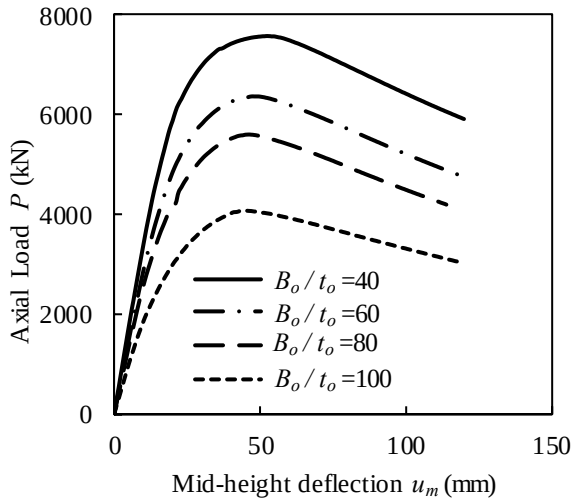

Fig. 13. Influences of B_o / t_o ratio on the axial load-deflection curves of square CFDST slender columns.

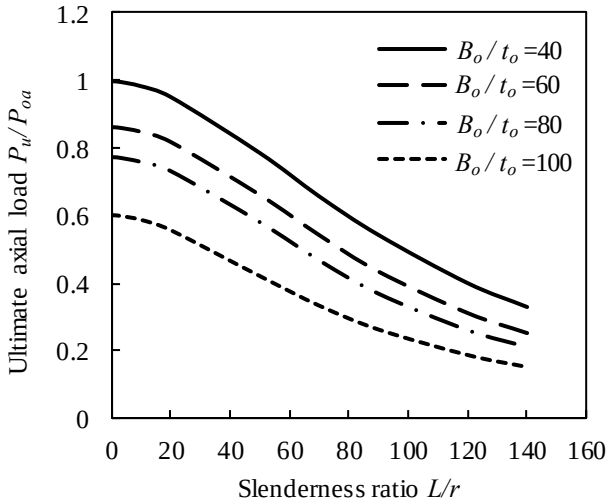

Fig. 14. Influences of B_o / t_o ratio on the column strength curves of square CFDST columns.

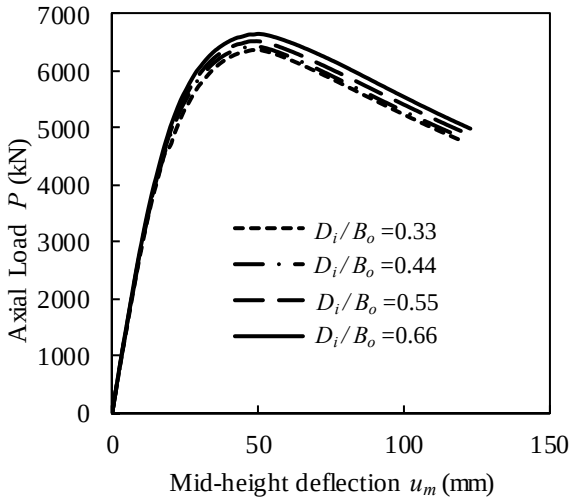

Fig. 15. Influences of D_i / B_o ratio on the axial load-deflection curves of square CFDST slender columns.

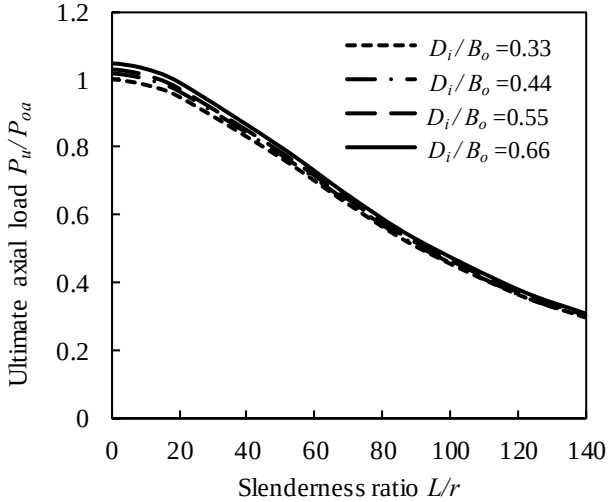

Fig. 16. Influences of D_i / B_o ratio on the column strength curves of square CFDST columns.

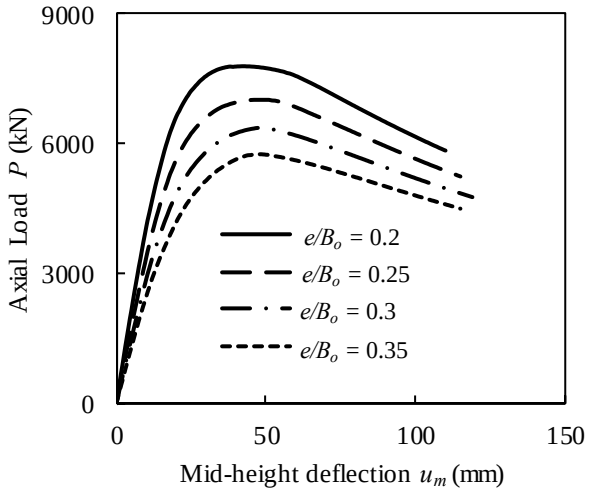

Fig. 17. Influences of e / B_o ratio on the axial load-deflection curves of square CFDST slender columns.

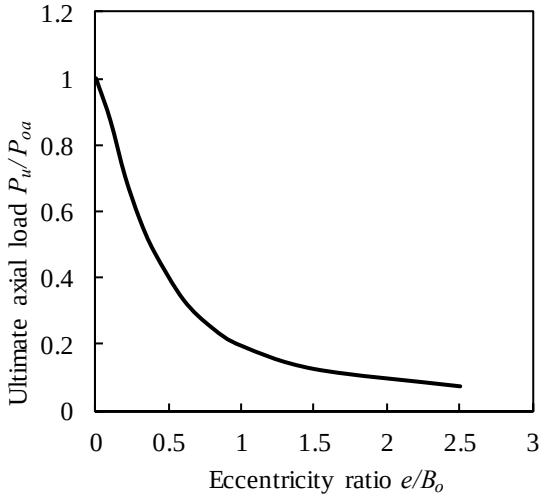

Fig. 18. Influences of e / B_o ratio on ultimate axial strengths of square CFDST slender columns.

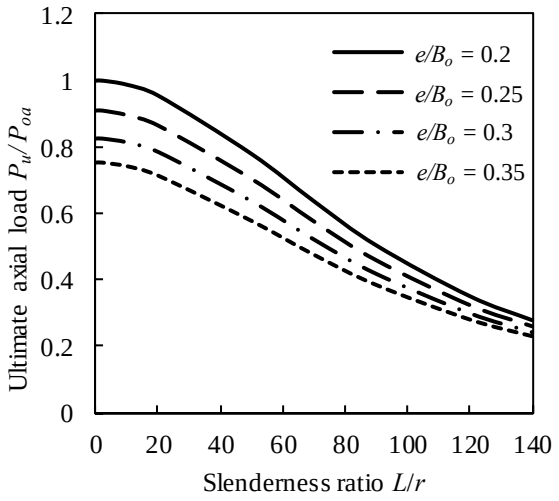

Fig. 19. Influences of e / B_o ratio on the column strength curves of square CFDST columns.

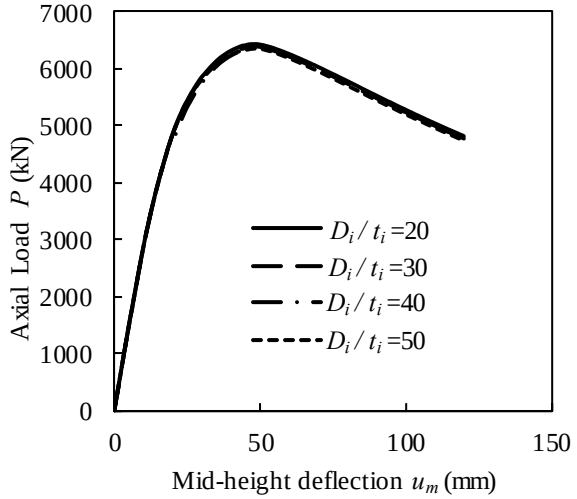

Fig. 20. Influences of D_i / t_i ratio on the axial load-deflection curves of square CFDST slender columns.

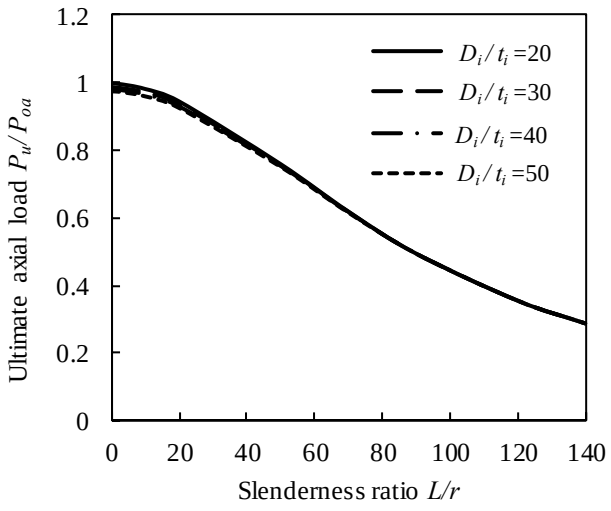

Fig. 21. Influences of D_i/t_i ratio on the column strength curves of square CFDST columns.

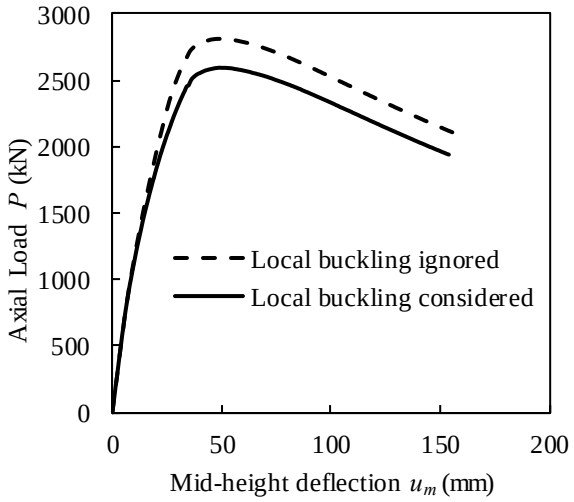

Fig. 22. Influences of the local buckling of outer steel tube on the axial load-deflection curve of square CFDST slender column.

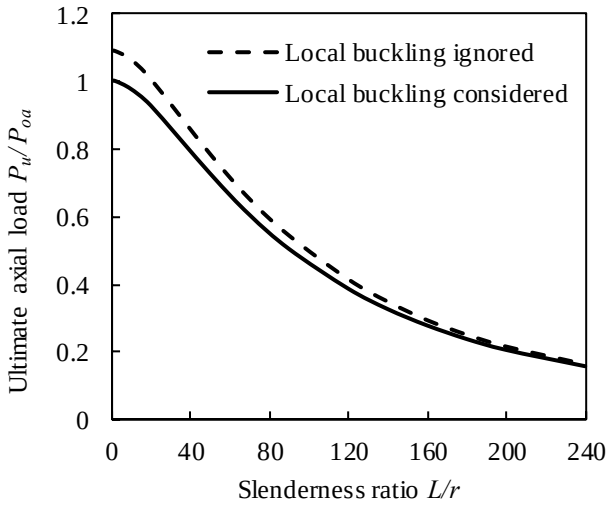

Fig. 23. Influences of the local buckling of outer steel tube on the column strength curves of square CFDST columns.

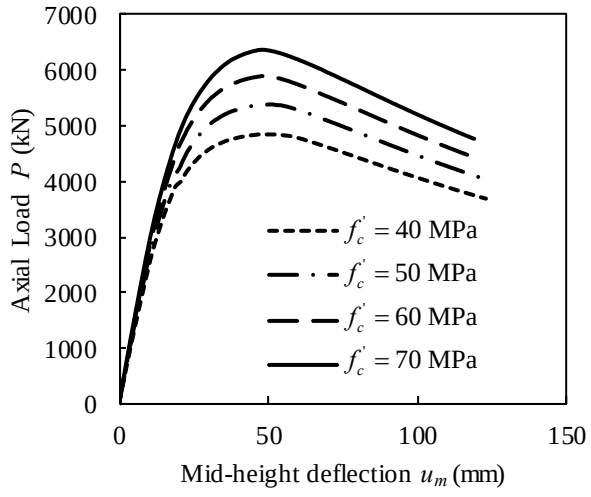

Fig. 24. Influences of concrete compressive strength on the axial load-deflection curves of square CFDST slender columns.

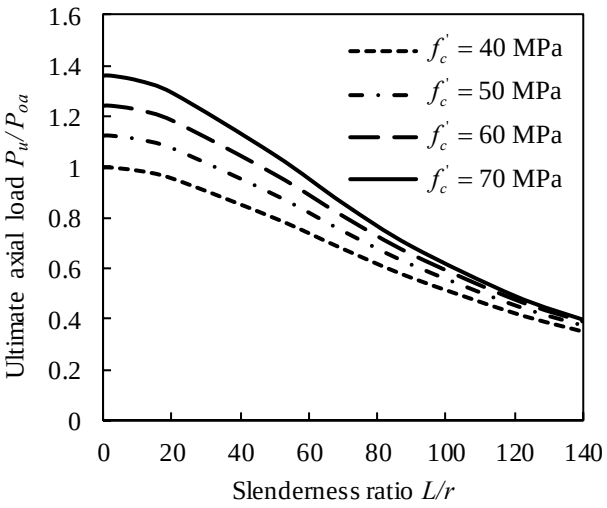

Fig. 25. Influences of concrete compressive strength on the column strength curves of square CFDST columns.

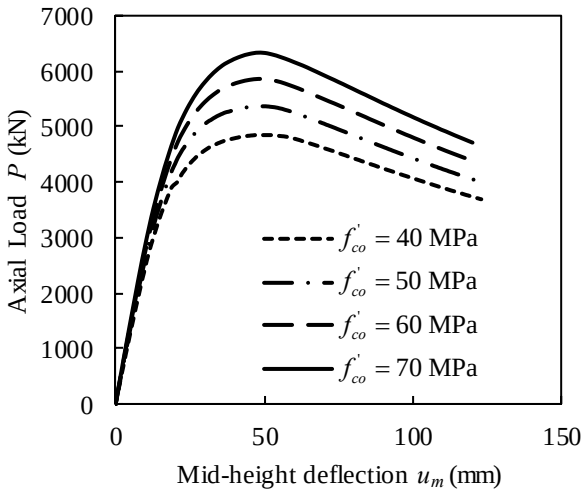

Fig. 26. Influences of sandwiched concrete strength on the axial load-deflection curves of square CFDST slender columns.

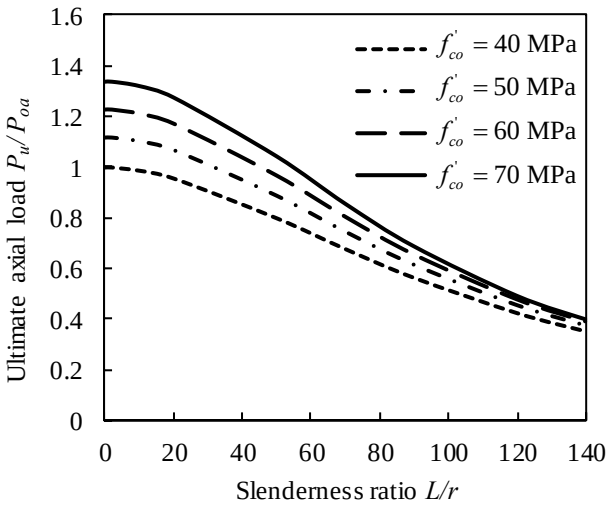

Fig. 27. Influences of sandwiched concrete strength on the column strength curves of square CFDST columns.

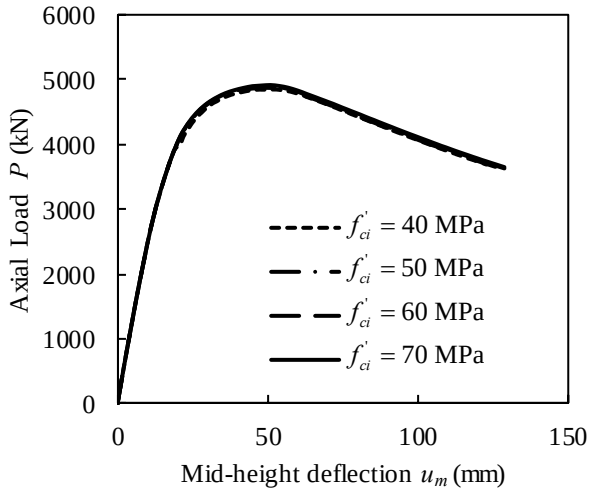

Fig. 28. Influences of core concrete strength on the axial load-deflection curves of square CFDST slender columns.

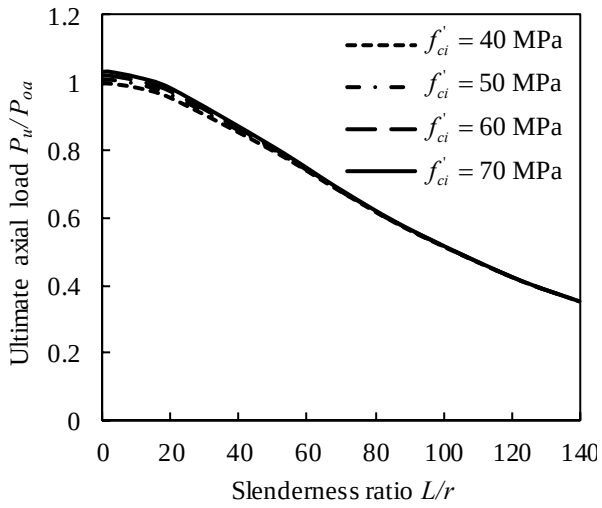

Fig. 29. Influences of core concrete strength on the column strength curves of square CFDST columns.

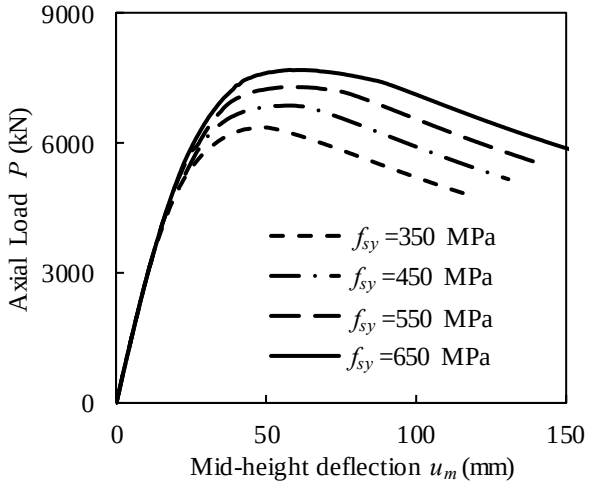

Fig. 30. Influences of steel yield strength on the axial load-deflection curves of square CFDST slender columns.

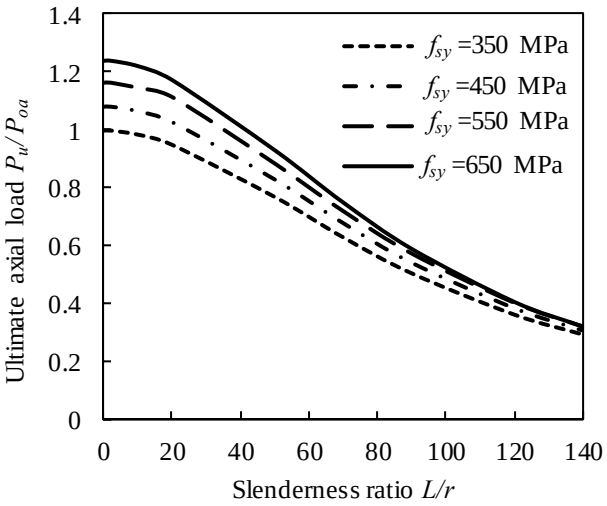

Fig. 31. Influences of steel yield strength on the column strength curves of square CFDST columns.

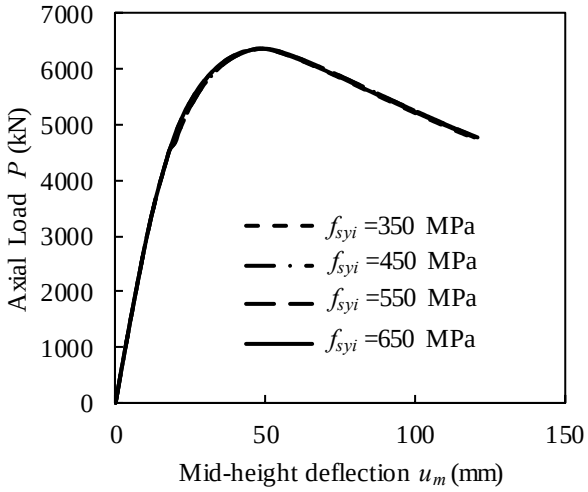

Fig. 32. Influences of steel yield strength of the inner steel tube on the axial load-deflection curves of square CFDST slender columns.

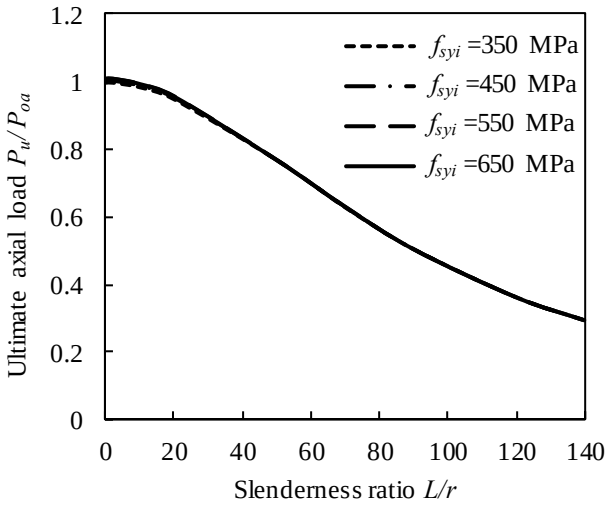

Fig. 33. Influences of steel yield strength of the inner steel tube on the column strength curves of square CFDST columns.

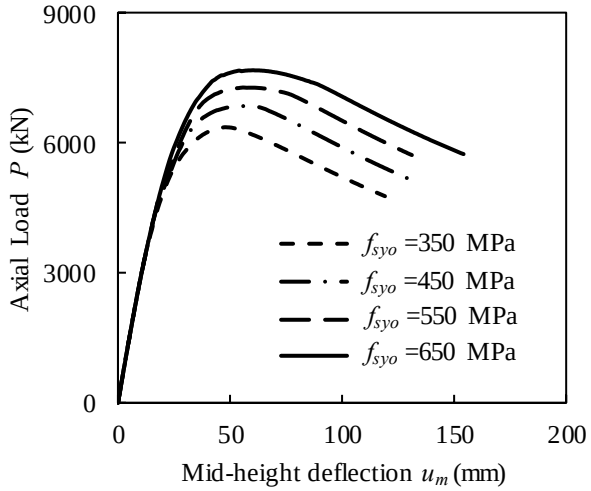

Fig. 34. Influences of steel yield strength of the outer steel tube on the axial load-deflection curves of square CFDST slender columns.

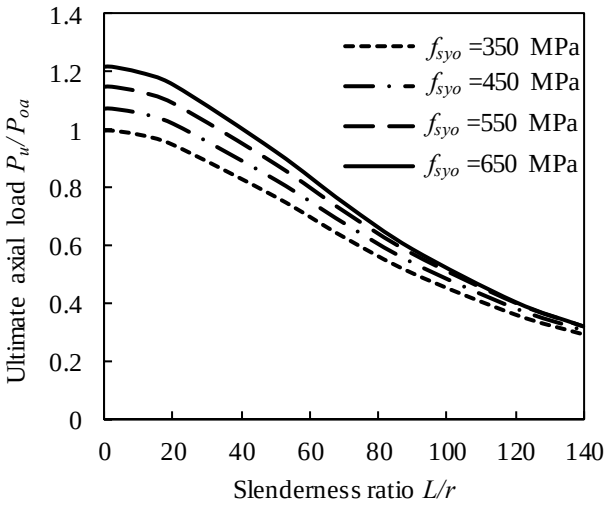

Fig. 35. Influences of steel yield strength of the outer steel tube on the column strength curves of square CFDST columns.

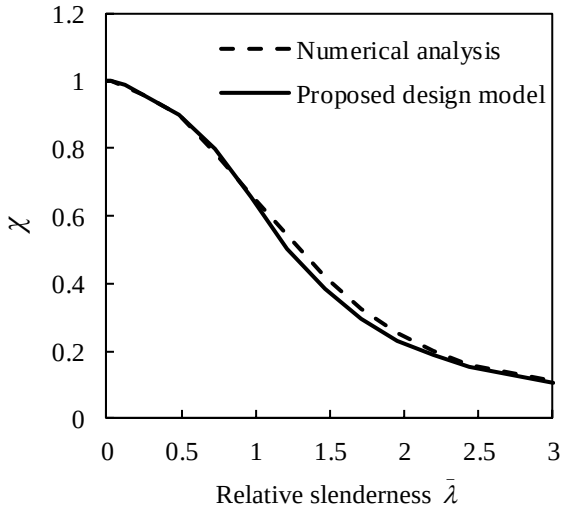

Fig. 36. Comparison of proposed design model with numerical analysis.

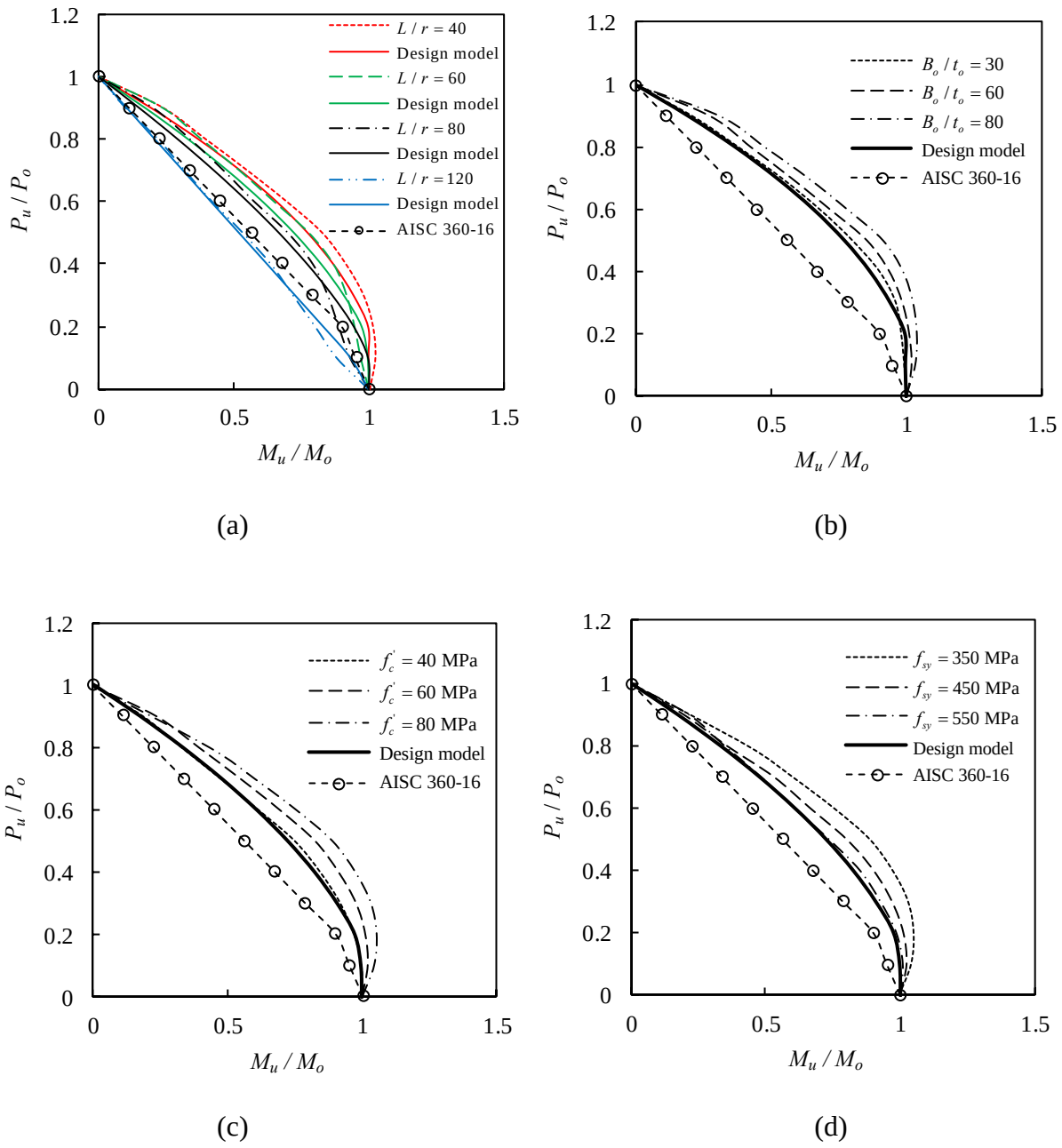

Fig. 37. Comparison of axial load-moment interaction curves for slender CFDST columns obtained by the proposed design equations and numerical model.